Title
Investigation of the hydrophobic/steric ratchet mechanism of the anthrax toxin φ clamp

Author
Colby, Jennifer

Publication Date
2012

Peer reviewed|Thesis/dissertation

Investigation of the hydrophobic/steric ratchet mechanism of the anthrax toxin ϕ clamp

by

Jennifer Moses Colby

A dissertation submitted in partial satisfaction of the

requirements for the degree of

Doctor of Philosophy

in

Molecular Toxicology

in the

Graduate Division

of the

University of California, Berkeley

Committee in charge:

Professor Bryan Krantz, Chair
Professor Chris Vulpe
Professor Susan Marqusee

Spring 2012

Investigation of the hydrophobic/steric ratchet mechanism of the anthrax toxin ϕ clamp

Abstract

Investigation of the hydrophobic/steric ratchet mechanism of the anthrax toxin ϕ clamp

by

Jennifer Moses Colby

Doctor of Philosophy in Molecular Toxicology

University of California, Berkeley

Professor Bryan Krantz, Chair

Transmembrane protein translocation is a fundamental and ubiquitous process that operates under several conserved principles. Protein conducting machines, known as translocase channels, catalyze the unfolding and subsequent transport of substrate proteins through narrow pores in an energy-dependent manner. Investigating how translocase machines rectify external energy inputs is key to understanding their force transduction mechanisms and overall function. Molecular ratchets are believed to be an integral mechanism for providing directional polypeptide transport through translocase channels, and several types of ratchets have been identified in these machines.

In this work, anthrax toxin, a protein translocase that possesses a hydrophobic gasket known as the ϕ clamp, is used as a model system to investigate the role of hydrophobic/steric ratcheting in protein translocation. Planar lipid bilayer electrophysiology was used to establish that the PA ϕ clamp binds hydrophobic/aromatic residues in peptide substrates, and to determine the consequences this binding interaction has on transport of these peptides. Under conditions where protein unfolding is shown to be rate-limiting, sequences identified as ϕ-clamp interacting increase translocation of folded downstream domains.

Single channel electrophysiology was used to record substrate and driving force dependent changes in the conductance of a single PA channel. Open, bound, and two intermediate conductance states are identified, which we hypothesize correspond to different conformations of the catalytic ϕ-clamp loop. Crystallographic evidence, which supports this theory, is presented. A kinetic analysis of single channel peptide binding and translocation events shows that the translocation pathway for hydrophobic/aromatic sequences has committed steps. A hydrophobic ratchet model is proposed to explain ϕ-clamp catalysis and how the favorable interaction between the clamp and hydrophobic/aromatic sequences may favor unfolding and increase directional movement of the translocating chain.

Table of Contents

List of Figures

List of Abbreviations

$\Delta\Psi$	membrane potential
ΔpH	proton gradient
ADP	adenosine 5'-diphosphate
ATP	adenosine-5'-triphosphate
cAMP	3'-5'-cyclic adenosine monophosphate
DTA	diphtheria toxin A chain
EDTA	ethylenediaminetetra acetic acid
EF	edema factor
ER	endoplasmic reticulum
LF	lethal factor
LF_N	amino-terminal domain of lethal factor
MAP	mitogen-activated protein
NAD^+	nicotinamide adenine dinucleotide
PMF	proton motive force; proton gradient
PA	protective antigen
PDB	protein data bank
SCB	single channel buffer
TCEP	tris (2-carboxyethyl)phosphine
UBB	universal bilayer buffer

Acknowledgements

My heartfelt thanks go out to everyone who has helped me throughout my graduate career. The list of people who have given me advice, training, and support is long; without you all I would not be where I am. For his scientific advice and mentoring, I would like to thank my advisor, Bryan Krantz. Bryan was instrumental in getting my project off the ground. Professor Len Bjeldanes was a great source of guidance and support during my early years, as were my fellow molecular toxicology students, Leona Scanlan and Hiro Satooka. I also thank my thesis and guidance committee members for their time and suggestions.

I am grateful to the members of the Krantz lab for their company and for thought-provoking conversation over the years: Mike Brown, Geoff Feld, Melinda Hanes, Alex Kintzer, Adam Schawel, Katie Thoren, and Sarah Wynia-Smith. Sarah and Melinda deserve special thanks as they mentored me extensively. Albert Lang was also instrumental in keeping me motivated and on track. My family, my husband Jake, and my horse Ty all provided moral support and kept me in good humor; both of which were essential for the completion of this thesis. Jake also kindly provided help with programming over the course of my graduate career.

This work was supported by the National Institutes of Health Research Grant R01-AI077703 (to Bryan Krantz), and the Berkeley Graduate Fellowship (to Jennifer Colby).

Chapter 1

Introduction to protein translocation

Proteins are widely regarded as the workhorses of the cell, carrying out the reactions that are necessary for life. The activity of a protein is contingent upon its three dimensional structure, as well as its localization. A properly folded protein that is improperly localized may be unable to function. Most proteins are synthesized in the cytosol and subsequently delivered to their sites of activity. Membrane-embedded proteins must be delivered to, and inserted into, the lipid bilayer. Secreted proteins, estimated to comprise almost a quarter of the prokaryotic proteome, must cross at least one membrane to reach the extracellular milieu (Driessen and Nouwen, 2008). Eukaryotic cells, which contain many membrane bound organelles, are estimated to move almost half of their proteins across a membrane (Schatz and Dobberstein, 1996; Wickner and Schekman, 2005). Transmembrane translocation of proteins is a fundamental but poorly understood cellular process.

Many small, lipophilic molecules can freely diffuse across membranes, small hydrophilic molecules have dedicated active and passive transporters (Lizák et al., 2008; Banks, 2009). The hydrophilic nature and sheer size of proteins precludes simple diffusion as a transport mechanism, and the vast number of different proteins that cross membranes eliminates the possibility of each protein having a cognate transporter. To facilitate the transmembrane flux of proteins, cells contain specialized membrane bound proteinaceous transporters, known as translocase channels. These molecular machines serve as conduits, chaperoning proteins from one side of the membrane to the other.

While translocation can occur co-translationally, such as in the eukaryotic endoplasmic reticulum translocon Sec61 and the prokaryotic plasma membrane SecY complex; many channels are capable of recognizing folded substrates (Schatz and Dobberstein, 1996; Osborne et al., 2005). In some cases, such as the bacterial twin-arginine transporter, the substrate protein is translocated in a folded form (Sargent, 2007). However, many translocase channels that recognize folded proteins have a narrow interior diameter, necessitating unfolding of substrate tertiary structure prior to passage through the channel (Falnes et al., 1994; Gmira et al., 2001; Lee and Schneewind, 2002). The coupling of protein unfolding and translocation is observed in bacterial toxins and secretion systems as well as in protein import to mitochondria and chloroplasts (Eilers and Schatz, 1986; Ruprecht et al., 2010; Murphy, 2011). Protein degradation machinery including the proteasome, a soluble protein complex that unfolds targeted proteins and feeds them into a proteolytic chamber; also exhibits translocase function (Sauer and Baker, 2011). Though translocase channels (which unfold their substrates) exhibit diverse morphologies and play varied cellular roles, they likely operate under common principles (Figure 1.1).

1.1 Substrate specificity

One hallmark of protein translocation machines is the lack of specificity inherent in their molecular mechanisms (Figure 1.2). While substrate selection does occur, it is largely independent of the unfoldase and translocase activities of the machine (Schatz and Dobberstein, 1996). The selection process can occur via direct binding to the translocase at a site other than the central pore, as is the case with many bacterial toxins and type III secretion systems. These channels have only a few substrates, so a direct binding interface is a simple way to select

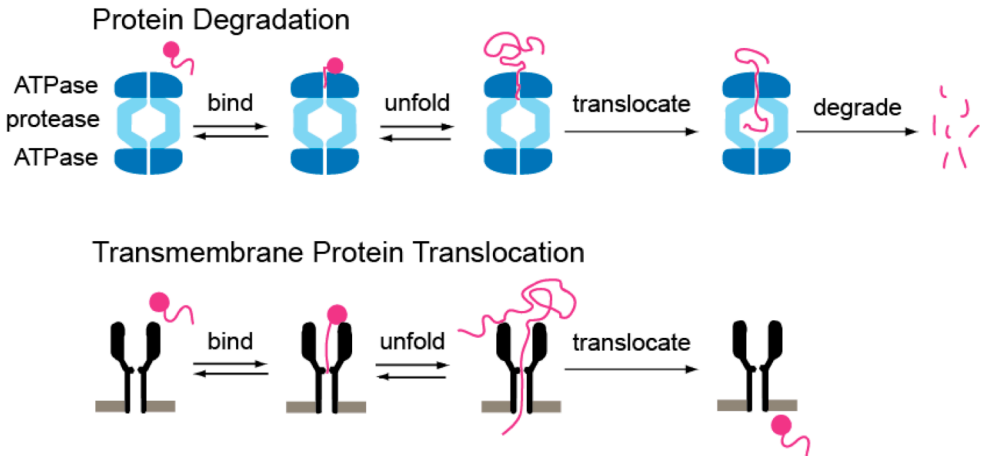

Figure 1.1. Common principles in protein transport. Protein degradation machines, which generally consist of a cylindrical proteolytic chamber (light blue) capped by ATPase rings (dark blue), must first bind their substrates (pink) via unstructured sequences. The ATPase motor then unfolds the substrate and translocates it into the proteolytic chamber for degradation. These same steps are involved in transmembrane protein translocation. The translocase channel (black) engages substrate (pink) via unstructured N-terminal sequences. The channel then unfolds the substrate and translocates it through a narrow pore and across the membrane. The substrate is free to refold after it has been released from the channel.

substrates. Non-natural substrates can be unfolded and translocated by these channels once they have engaged the pore machinery (Wesche et al., 1998; Chen et al., 2006; Holubova et al., 2012). Typically, threading an unfolded sequence into the pore is enough to initiate transport, and this is often accomplished in vitro by fusing model domains to binding domains of the natural substrates.

Machines with more numerous substrates, like the proteasome and related degradation machinery, use specific signal tags known as degrons to identify their substrates (Striebel et al., 2010; Sauer and Baker, 2011). Thousands of proteins of varying size, structure, and thermodynamic stability are recognized via degrons, then unfolded and translocated into the degradation machinery by these machines (Kenniston et al., 2003; 2004; Barkow et al., 2009). Similarly, about one thousand different proteins are targeted to the mitochondria by a presequence that is recognized by the import machinery (Pfanner and Geissler, 2001). Given the sheer number of different proteins that are unfolded and transported by translocase channels, the isolation of substrate selection from further processing steps allows translocase function to be conserved without compromising substrate selectivity.

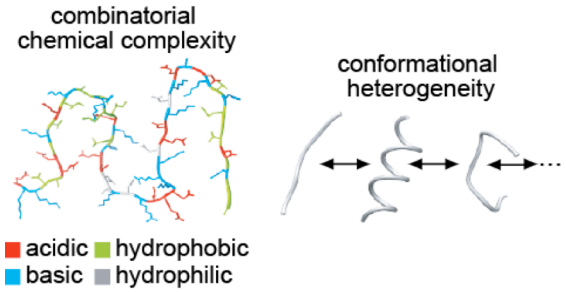

Figure 1.2. Translocases process diverse substrates. The fundamental mechanisms of protein translocation are non-specific. Translocase channels are able to interact with substrates of varying secondary structure and amino acid composition. Substrate selection occurs via tags or specific binding sites. Illustration adapted from Thoren and Krantz, 2011.

1.2 Energetics

All translocation of proteins across lipid bilayers requires energy; however, the driving force, and how it is harnessed, varies. Chemical energy, in the form of nucleotide triphosphates, or electrochemical gradients are used to power cellular translocases (Simon et al., 1992). Translocases can be classified as active or passive based on the role the channel plays in energy capture and transduction of force to the substrate.

Passive channels like the mitochondrial protein import system and the Sec61/SecY complexes do not directly utilize energy, rather they associate with force producing proteins. Binding and hydrolysis of GTP by ribosomes and other associated proteins provides the energy for co-translational translocation (Finke et al., 1996; van den Berg et al., 2004; Jiang et al., 2008). Ribosomes that have begun synthesizing secreted or membrane proteins use a multi-protein scaffold system to associate with an ER translocon; the continued addition of amino acids to the C-terminus pushes the nascent chain through the pore (Park and Rapoport, 2011a). In the case of import into mitochondria, Hsp (Heat shock protein) motor proteins use energy derived

from ATP binding and hydrolysis to interact processively with translocating substrates. Iterations of substrate binding and release by Hsps promotes unfolding by stabilizing the unfolded structure and facilitates translocation, largely by preventing retrograde movement of the polypeptide chain (Liu et al., 2003; Yamano et al., 2008). Post-translational translocation at the eukaryotic ER translocon is also driven by ATP binding and hydrolysis in the form of an Hsp binding and release mechanism (Park and Rapoport, 2011a).

In contrast, active translocase channels are able to directly use energy to do work on substrates. The translocase components of many protein degradation machines are members of the AAA+ (ATPases Associated with diverse cellular Activities) superfamily (Sauer and Baker, 2011). AAA+ translocases are hexameric, ring shaped complexes, that bind and hydrolyze ATP to power protein unfolding and subsequent translocation into the associated degradation chamber. Binding of ATP at just one of the six subunits is enough to power the machine, though maximal efficiency is observed when ATP is bound at four subunits (Martin et al., 2005; Glynn et al., 2009). From this starting state, translocation is powered by cycles of hydrolysis of 1 bound ATP, followed by release of ADP and binding of a new ATP, with the process proceeding through each of the subunits (Glynn et al., 2009). The amount of ATP used, and the efficiency with which energy is coupled to translocase activity depends on the translocase as well as the substrate protein (Herman et al., 2003; Kenniston et al., 2003; Kwon et al., 2004; Choy et al., 2007).

Active translocases can also be powered by the proton motive force (PMF). Rather than using chemical energy stored in molecules, these proteins use energy from electrochemical gradients to power unfolding and translocation. The two components of the PMF rely on unequal H+ concentration across a membrane; one component is a simple chemical gradient of ions, the other is a membrane potential that is established by unequal distribution of charges. Translocase channels from the pathogenic bacteria *Bacillus anthracis* and *Corynebacterium diptheriae* use the PMF to intoxicate host cells (Krantz et al., 2006; Basilio et al., 2009; Brown et al., 2011; Murphy, 2011). Secretion of flagellar proteins by the bacterial type III secretion system is also accomplished through use of the PMF (Minamino et al., 2011). Channels that use the PMF are often considered protein-proton symporters (Krantz et al., 2006; Finkelstein, 2008; Basilio et al., 2009).

Whether it is extracted from chemical bonds or ion gradients, the end result is the same; protein transport requires energy. All active translocase channels directly use energy to unfold their substrates and translocate the resultant polypeptides; all passive translocase channels rely on auxiliary proteins to harness energy. Despite divergences in how the energy source is coupled, both active and passive channels employ broad, well conserved, mechanisms to transduce force to substrates.

1.3 Force transduction mechanisms

Translocase channels can be likened to molecular motors traveling along a polypeptide track. Motors, including these molecular machines, are energy converters; energy put into the motor creates a mechanical output. As I have discussed at length in section 1.2, translocase channels or associated proteins extract energy from chemical bonds or electrochemical gradients. The energy is subsequently used to power substrate unfolding and passage through the channel. This section will focus on two broad mechanisms that describe how translocase channels and associated proteins convert energy into mechanical force that is applied to their substrates.

Energy is transduced to the substrate either by a concerted power stroke, by a ratcheting

mechanism, or through a combination of these (Figure 1.3). The power stroke model entails the motor pushing or pulling on the substrate, resulting in unfolding and translocation through the channel. Ratchet models, of which there are several varieties, describe the motor as biasing diffusive Brownian motion and preventing retrograde translocation using energy from an external gradient. The power stroke and ratchet models have been applied to active channels and to motor proteins associated with passive channels, and are not mutually exclusive (Alder and Theg, 2003; Hwang and Lang, 2009).

Translocases and motors that bind ATP are thought to transduce force to their substrates via a power stroke. In the case of AAA+ motors, like the bacterial proteasome ClpXP, nucleotide dependent conformational changes in pore loops that contact substrate are thought to physically push on the substrate (Glynn et al., 2009; Aubin-Tam et al., 2011). Each cycle of ATP binding and hydrolysis pushes the pore loops down, which pulls on the substrate, and then the loops are reset to the original conformation. In order to do work, the resetting must occur through a different pathway than the power stroke (Glynn et al., 2009; Sauer and Baker, 2011). Ultimately substrate unfolding would be achieved by the applied pulling force and coincident transient stochastic destabilization of the substrate (Aubin-Tam et al., 2011). Already unfolded regions could then be easily fed through the pore and into the degradation chamber. The power stroke model describes machines that run on chemical energy well, but is not sufficient to describe machines that use gradients.

Many translocation machines that derive energy from electrochemical gradients are thought to function as Brownian ratchets (Tomkiewicz et al., 2007). In this mechanism the machine actively biases random thermal fluctuations, or Brownian motion, of the substrate to move the chain through the channel. A molecular pawl, a part of the channel that prevents retrograde translocation, biases the motion. The key difference between the power-stroke model and the Brownian ratchet is how the machine generates the force that it applies to the substrate. Power-stroke machines generate force from ATP binding and hydrolysis and apply it to the substrate; Brownian-ratchet machines bias an external energy source to translocate the substrate. While power-stroke machines directly convert chemical energy into mechanical work, Brownian-ratchet machines exploit external gradients.

All Brownian ratchets operate under the same basic principle, but the type of pawl that is used to create directionality varies. Three main types of pawls have been proposed; one operates on charge exclusion, another on hydrophobic/steric binding, and the last by steric clamping. Charge-state ratchets rely on a pH gradient across the membrane and a charge-selective channel (Krantz et al., 2006). Selective protonation of acidic residues in the substrate on the low-pH side of the membrane would allow the chain to enter a cation selective channel. When the chain has reached the higher-pH side of the membrane, the protons would be released, leaving an anion that would be repulsed by the cation-selective channel. In this case, the pawl is comprised of the charge-exclusion sites in the channel (Brown et al., 2011; Krantz et al., 2006).

Hydrophobic/steric ratchets rely on a favorable interaction between exposed hydrophobic loops in the channel and hydrophobic/aromatic residues in the substrate. This interaction could stabilize partially unfolded substrates, and prevent retrotranslocation through steric hindrance between the bulky pore loop and the recently translocated sequence (Krantz et al., 2005; Thoren et al., 2009; Aubin-Tam et al., 2011). Generally, the core of a folded substrate protein is hydrophobic, while the interior of a translocase channel is largely hydrophilic. By offering a stable hydrophobic binding site in the lumen, the channel can capture unfolded states of the substrate that would otherwise be unstable, and help drive unfolding. Bulky, hydrophobic

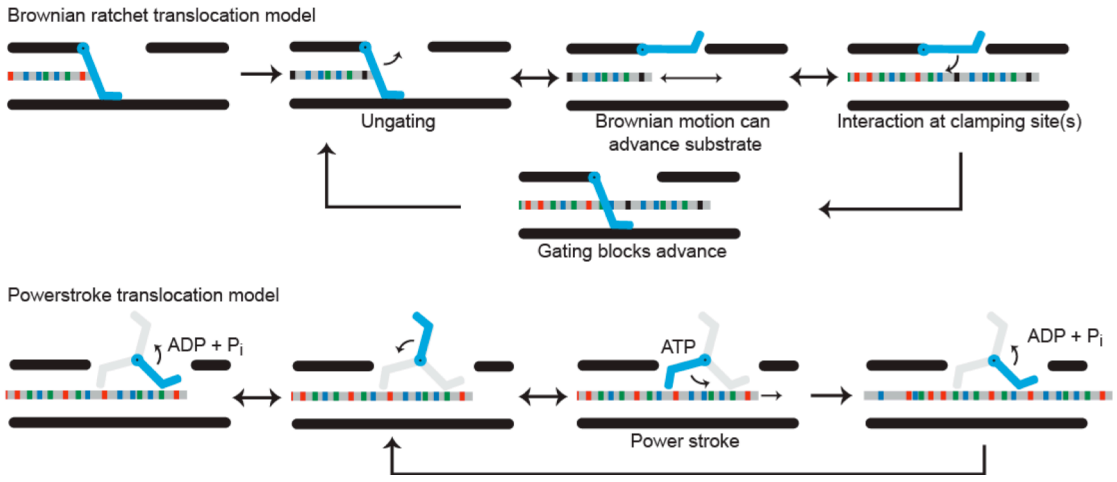

Figure 1.3. Force transduction in protein translocation. Two main mechanisms of force transduction have been proposed to describe how translocases move substrates: ratchet and power stroke. Ratchet machines bias Brownian motion, as shown in the top schematic. The bias is initiated by a clamping structure in the machine that acts as a molecular pawl to prevent retrograde movement. The clamp, shown here in cyan, allows movement of the substrate in one direction but engages and prevents movement in the opposite direction. Clamping can be charge state dependent, requiring a proton gradient and a charge exclusion site in the channel, or hydrophobic. In the power stroke, shown on the bottom panel, the translocase uses conformational changes from ATP binding and hydrolysis to actually push or pull on the substrate to move it through the channel. The force is applied to the substrate by a pore loop, shown in cyan. Illustration adapted from Feld *et al.*, 2012.

residues that have translocated beyond the hydrophobic pore loop are unlikely to retrotranslocate if the driving force should temporarily subside, due to steric exclusion at the loop site. Thus the loop is acting as a ratchet pawl, biasing movement in one direction. Once the chain has exited the channel it can begin refolding, reducing the entropic costs of ordering water around hydrophobic residues.

In the steric-clamping ratchet, a gradient of binding proteins across the membrane provides directionality (Simon et al., 1992). If in addition to a concentration gradient, these proteins have a high affinity for unfolded structure, they will primarily bind to proteins as they exit the channel, thus further biasing the motion. Steric clamping has mainly been proposed for systems with passive channels, like the mitochondrial import system (Liu et al., 2003; Yamano et al., 2008).

As an example of the complementarity of the power stroke and ratchet models, the Hsp70 mitochondrial import motors have ATPase activity and are also thought to push and pull on substrates in an ATP dependent fashion, similar to AAA+ motors. It has been proposed that nucleotide dependent conformational changes in the Hsps are converted to mechanical force by an interaction at the import channel. The dual interactions with channel and substrate would allow Hsp70 to act as a lever and pull on the substrate (Matouschek et al., 2000). The unified entropic-pulling model, which incorporates elements of both ratchets and power strokes, was proposed to explain the dual nature of Hsp70 force transduction. In this model Hsps in the matrix use energy from ATP to apply a pulling force on the incoming protein while simultaneously biasing motion though steric clamping effects (De Los Rios et al., 2006). Entropic pulling allows for Hsp70 to act either via a ratchet or via a power stroke depending on the number of Hsp70 binding sites available in the substrate (Goloubinoff and De Los Rios, 2007). There is a strong possibility that other translocase channels will display elements of both the power-stroke and ratchet models, and a simple combination of the two models might best describe their mechanisms (Aubin-Tam et al., 2011; Brown et al., 2011).

1.4 Hydrophobic pore rings & substrate interactions

Both the power-stroke and hydrophobic/steric-ratchet models rest on the channel possessing a hydrophobic pore loop. Unsurprisingly, these structures are found in a great number of translocase channels (Krantz et al., 2005; Erlandson et al., 2008; Martin et al., 2008; Park and Rapoport, 2011b; Sauer and Baker, 2011). The ubiquitous nature of these pore loops, or hydrophobic/aromatic clamping sites, indicates their importance in the mechanism of protein translocation. They can catalyze translocation directly or indirectly and they can help maintain gradients across cellular membranes.

Each subunit of the hexameric AAA+ family of translocases contributes three residues to form the hydrophobic pore loop the machines use to grip substrates. The sequence is well conserved, with the pattern being aromatic-hydrophobic-glycine (Sauer and Baker, 2011). In the proteasome ClpXP, the contact made between the tyrosine/valine sequence in the translocase pore loop and the substrate is what allows the power stroke to produce force (Martin et al., 2008). Mutation of the pore loop residues in even two of the six subunits is enough to kill activity of the machine (Martin et al., 2008). Other translocases, including bacterial toxins, also make use of catalytic pore loops. Anthrax toxin, which contains an active translocase channel component as well as cytotoxic substrates, has a ring of catalytic phenylalanine residues in the channel lumen. This hydrophobic clamp structure has been implicated in substrate unfolding and

translocation, and is quite sensitive to mutation (Krantz et al., 2005; Thoren et al., 2009; Janowiak et al., 2010).

Hydrophobic pore loops are also found in passive channels and in the associated motor proteins. The bacterial plasma membrane translocase, SecY, associates with the cytoplasmic motor protein, SecA to translocate substrates post-translationally (Park and Rapoport, 2011a). In a mechanism quite similar to that of ClpX, SecA converts the energy from ATP binding and hydrolysis to a pushing motion on the substrate, forcing substrate through the channel (Erlandson et al., 2008). The contacts between SecA and the substrate map to a loop, and the active residue is an aromatic, Tyr (Erlandson et al., 2008). SecY itself has an hydrophobic pore ring that is critical in maintaining the gradients across the membrane (van den Berg et al., 2004; Park and Rapoport, 2011b). When the channel is inactive, the pore is filled with a protein plug, which prevents the movement of ions and small molecules. When the channel is active the pore ring forms a tight seal around the translocating polypeptide, acting as a molecular gasket to prevent leakage. Other transporters also contain hydrophobic pore rings that are important in interacting with substrates (Schirmer et al., 1995).

1.5 Questions

We know that many translocases interact with substrates via hydrophobic pore loops, but how the interactions promote translocation is poorly understood. How do translocases process substrates with differing primary sequence? Do hydrophobic pore loops function as hydrophobic/steric ratchets? How do machines balance the thermodynamic stability of substrate-loop complexes with kinetic concerns? These questions are best addressed in a model system where the substrate and the driving force can be precisely controlled. Anthrax toxin, which I will use in this thesis, fulfills these requirements.

1.6 Anthrax toxin as a model translocase

Bacillus anthracis, the pathogenic bacterium responsible for many livestock deaths, secretes a tripartite virulence factor known as anthrax toxin. The toxin is classified as an A-B toxin; these types of toxins have an active (A) component and a binding or delivery (B) component. Anthrax toxin has two distinct active components and one binding component. The active component lethal factor (LF) is a ~90 kDa zinc-dependent metalloprotease that cleaves mitogen activated protein kinase kinases (Duesbery et al., 1998). The second active component, edema factor (EF) is a ~90 kDa calcium/calmodulin dependent adenylate cyclase that raises intracellular levels of the second messenger cAMP (Leppla, 1982). Together LF and EF alter cellular signaling which eventually results in cell death. The B component of anthrax toxin is formed by a seven to eight membered oligomer of protective antigen (PA) (Milne et al., 1994; Petosa et al., 1997; Katayama et al., 2008; Kintzer et al., 2009) (Figure 1.4).

PA, named for its ability to provide immunity against further anthrax infection in inoculated animals, is secreted by the bacillus as an 83 kDa monomer. Subsequent cleavage by proteases in the host results in a 63 kDa fragment that is able to form a homo-oligomer (Ezzell and Abshire, 1992; Milne et al., 1994; Mabry et al., 2006; Kintzer et al., 2009). PA oligomers bind cargo, about three or four molecules of LF or EF. The assembled toxin complexes bind to receptors on the surface of host cells. Through receptor mediated endocytosis, the fully assembled anthrax holotoxin is delivered to endosomes. As the endosome is trafficked though the cell, it is acidified. The change in pH has three important consequences. First, it triggers a conformational change in the PA oligomer, as a result the oligomer inserts into the endosomal

membrane and forms an active translocase channel (Blaustein et al., 1989; Miller et al., 1999). Second, the low pH destabilizes the tertiary structures of LF and EF (Krantz et al., 2004). Finally the low pH in the endosome, relative to the neutral conditions in the cytosol, establishes a proton gradient (or PMF), across the endosomal membrane. PA then uses both electrical and chemical components of the PMF to unfold LF and EF and translocate them from the endosome to the cytosol (Zhang et al., 2004a; Krantz et al., 2005; 2006; Thoren et al., 2009; Brown et al., 2011).

The translocation mechanisms proposed for PA share many salient features with other translocases, including AAA+ motors. PA is thought to function primarily through ratchet mechanisms, both charge-state and hydrophobic/steric (Krantz et al., 2005; Thoren et al., 2009; Feld et al., 2010; Brown et al., 2011; Feld et al., 2012) (Figure 1.5). The charge state ratchet, described in more detail in section 1.3, operates on a pH gradient and is likely to be the primary mechanism in vivo (Zhang et al., 2004b; Thoren et al., 2009; Brown et al., 2011). However, PA can actively translocate substrates in the absence of a ΔpH, so this model does not account for all of the channel's activity.

Like AAA+ motors, PA contains a hydrophobic pore loop, termed the ϕ clamp, that catalyzes translocation (Krantz et al., 2005). Each PA subunit contributes a phenylalanine to form the clamp, which is situated at the most narrow site inside the channel, and forms a tight seal around the translocating sequence (Krantz et al., 2005; 2006; Sun et al., 2008). The ϕ clamp, which is known to bind hydrophobic-aromatic cations, has been hypothesized to act as a hydrophobic/steric ratchet site (Krantz et al., 2005). The ϕ clamp is thought to interact favorably with hydrophobic and positively charged residues that would be exposed as the substrate unfolded. The ϕ clamp would then catalyze translocation by binding the substrate and stabilizing it in partially unfolded states and by preventing retrograde translocation (Krantz et al., 2005; Thoren et al., 2009; Feld et al., 2012). To date, no evidence has been presented to support a power-stroke model of PA translocation, but neither has it been excluded.

PA also contains a helix-binding motif, the α clamp, that catalyzes substrate unfolding (Feld et al., 2010; Thoren and Krantz, 2011). The α clamp, which binds amphipathic helices, is able to interact with many different kinds of sequences. Similar helical-binding motifs have been identified in other protein chaperones (Street et al., 2011). Sites like the α clamp and ϕ clamp, that recognize general structures or features of the polypeptide, may explain why translocase channels can process such a great diversity of combinatorially and chemically complex substrates (Figure 1.2).

There are many distinct advantages to using anthrax toxin as a model translocase channel. As I have discussed, PA shares structural and mechanistic details with other translocase systems. PA has been cloned and can be expressed recombinantly, independent of LF and EF. PA oligomers have a stable soluble form that can insert into artificial lipid bilayers and form a cation-selective translocase channel (Blaustein et al., 1989; Zhang et al., 2004a; 2004b; Krantz et al., 2005). An externally-applied electrical potential or pH gradient is sufficient to drive translocation of effector proteins in the artificial system, no auxiliary cellular factors are required (Wesche et al., 1998; Brown et al., 2011). PA can also translocate non-natural substrates, provided they have a positively-charged sequence at the N-terminus (Blanke et al., 1996; Wesche et al., 1998; Collier, 2009). Using electrophysiology we can measure single channel and ensemble translocations, and we can precisely control the driving force applied to the substrate (Figure 1.6). Ultimately, it is these factors, and the knowledge that PA exhibits conserved catalytic mechanisms, that guide our decision to use PA as a model translocase.

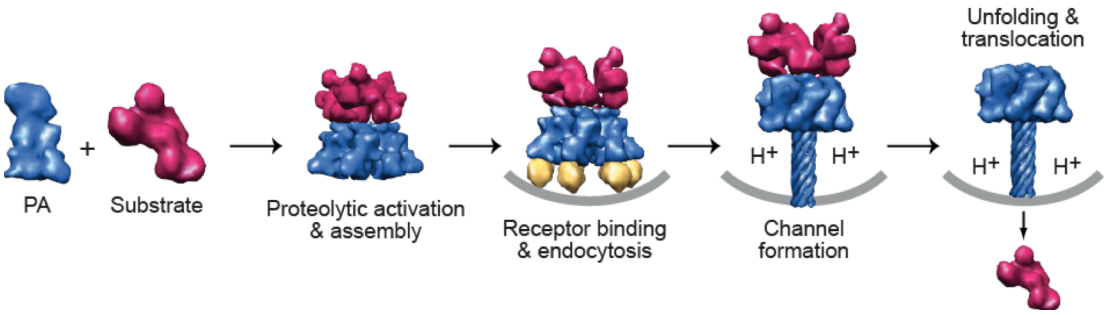

Figure 1.4. Anthrax toxin assembly and translocation. Protective antigen (PA) and substrates (LF and EF) are secreted by *B. anthracis* as monomers. Following proteolytic activation, PA assembles into a ring shaped oligomer and binds substrates, forming a holotoxin. PA binds receptors on the surface of the cell, triggering endocytosis. As the endosome is acidified, the low pH triggers a conformational change in PA, allowing channel formation, as well as destabilization of substrate proteins. PA then uses the pH gradient and membrane potential across the endosomal membrane to power translocation. PA catalyzes substrate unfolding and translocation. Substrates refold and regain their toxic activities when they reach the cytosol. Illustration adapted from Feld *et al.*, 2012.

1.7 A tunable hydrophobic/steric ratchet may drive protein translocation

In this thesis I will explore the details of how hydrophobic/steric ratchets function in PA catalyzed protein translocation. Based on previous results with a small molecule library, we hypothesized that PA's ϕ clamp would bind hydrophobic/aromatic residues in substrates (Krantz et al., 2005; Feld et al., 2012). Furthermore we predicted that this favorable interaction would 'pause' translocation, leading to slower translocation of densely hydrophobic/aromatic regions. These hypotheses have been presented numerous times in the literature but they have not been directly addressed in any previous work. In Chapter 2 I present the results of experiments to determine how small peptide probes bind to the channel and the results of single molecule kinetic experiments that address whether favorable interactions at the ϕ clamp lead to slower translocation. In Chapter 3 I present crystallographic and electrophysiological evidence that the ϕ clamp can adopt multiple conformations, and that these conformations represent committed steps in the translocation pathway. This thesis presents evidence to support the hypothesis that the ϕ clamp binds hydrophobic/aromatic residues in substrates and acts as a hydrophobic/steric ratchet to promote protein unfolding and translocation. The multiple ϕ-clamp conformations that we have discovered could provide a basis for how the channel maintains the kinetic-thermodynamic balance to favor unfolding without limiting translocation. We propose that the different ϕ-clamp loop conformations have different substrate affinity, and that the channel might regulate the degree of substrate interaction in a driving force-dependent manner. In this model, when driving force increases, the channel would release substrate for productive translocation; when the driving force subsides, affinity for substrate would increase, thus preventing the substrate from retrotranslocating. I believe the mechanisms proposed here are likely to be generalizable to other translocases with hydrophobic/aromatic pore loops.

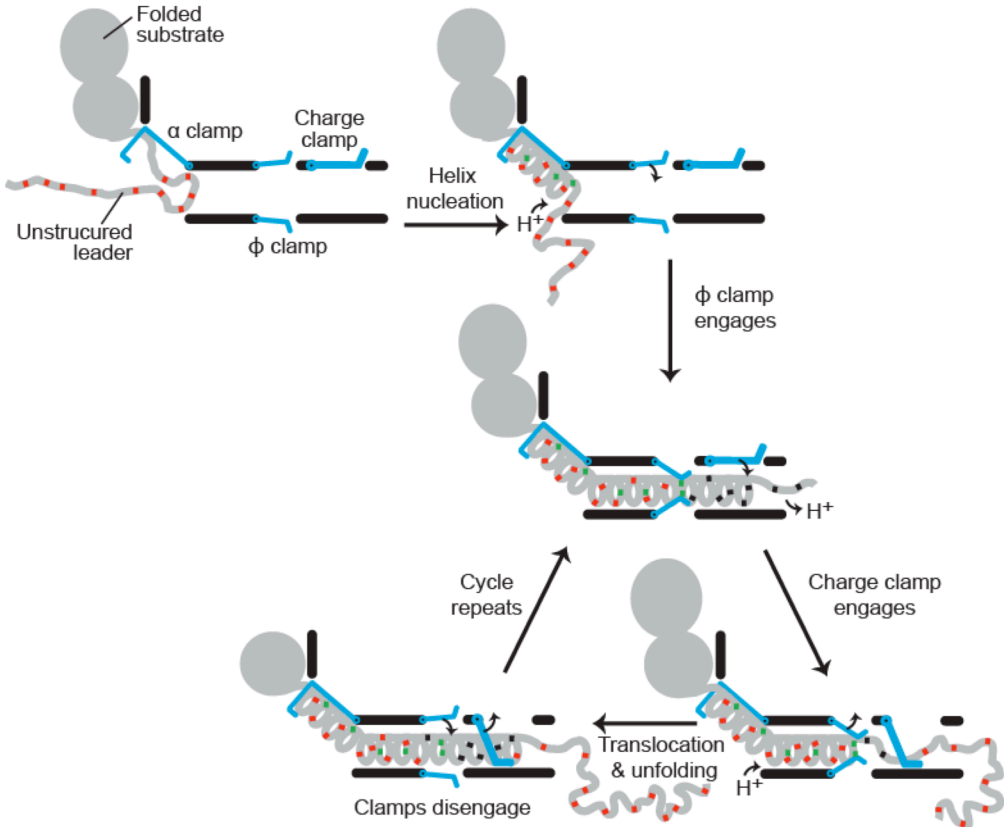

Figure 1.5. Ratchet driven translocation in PA. The three important PA clamping systems are shown in cyan. The α clamp, which binds helices, is important for unfolding substrates. The ϕ clamp, which we propose binds hydrophobic/aromatic sequences, is an important hydrophobic clamping site. We propose that the ϕ clamp has a tunable affinity for substrates, as indicated by the engaged and disengaged conformations. The final clamp is a charge-exclusion site that operates on a PMF and prevents retrograde movement of negatively charged residues. We believe that synergy between these 3 clamping systems drives substrate unfolding and translocation in anthrax toxin. Illustration adapted from Feld *et al.*, 2012.

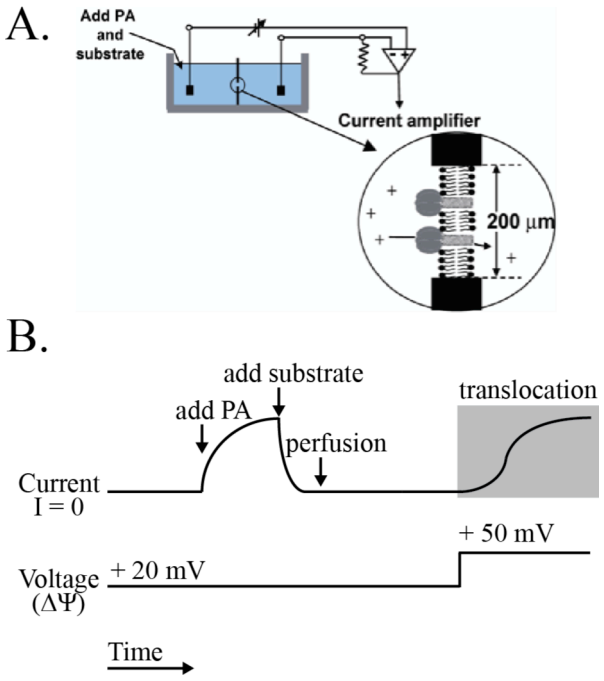

Figure 1.6. Planar lipid bilayer electrophysiology is used to monitor PA translocation. (A) Diagram of our instrument setup. **(B)** Typical recording of a voltage driven translocation experiment. A bilayer is formed by painting a lipid solution over a small hole in a plastic partition (labeled 200 μM in A). Symmetric electrolytic solutions are added to either side of the partition. PA, the channel-forming protein, is added to the front chamber of the apparatus and it inserts into the membrane. As PA is a cation-selective channel, we can measure current and watch in real time as channels insert into the membrane. A substrate protein is then added to the front chamber, where it binds the channels, and consequently blocks current. Excess substrate is removed via perfusion. In this schematic, translocation is initiated by increasing the applied voltage. Changes in current, as indicated by the gray box, allow us to monitor translocation in real time.

Chapter 2

Investigating substrate selection and engagement at the ϕ clamp

2.1 Introduction

Many processes critical for cellular viability depend on a group of molecular machines known as translocase channels. Translocases, which exist in soluble and membrane bound forms, often have a small interior diameter, which necessitates the unfolding of substrates prior to passage through the pore. These machines actively interact with unfolded chains during the transport process, using conserved mechanisms of translocation. Translocases often have a ring of hydrophobic/aromatic residues located at the constriction point within the pore. Known as a ϕ clamp or hydrophobic gasket, these residues are critical for efficient unfolding and translocation of substrate proteins. Mutations at these sites greatly reduce or even abolish activity, illustrating that the translocase directly interacts with the substrate via these loops (Krantz et al., 2005; Martin et al., 2008).

Generally, hydrophobic pore loops are thought to function as power stroke force transducers or ratchet pawls, or some combination of the two. Anthrax toxin's protective antigen (PA) possesses a phenylalanine clamp (ϕ clamp) that is hypothesized to catalyze translocation by acting as a hydrophobic ratchet (Krantz et al., 2005; Feld et al., 2012). Hydrophobic/steric ratchets are thought to assist substrate unfolding and play a role in directional propagation of substrate. A tight interaction at the ϕ clamp would stabilize a partially unfolded substrate, but it would also pose a barrier for further translocation. Clamps must have a tunable affinity mechanism that balances kinetics and thermodynamics, providing enough stability to lower the unfolding barrier, but not so much as to limit translocation. Though the hydrophobic/steric ratchet mechanism has been proposed many times, there is little evidence in the literature to explain how clamps select, engage, and disengage substrate sequences (Feld et al., 2012). In this chapter, I will address how the ϕ clamp selects substrates and the functional consequences of substrate engagement.

Here we investigate the interactions between peptide probes, model multi-domain substrates, and the PA ϕ clamp; focusing on kinetic and thermodynamic analysis. We hypothesize that the ϕ clamp will display substrate specificity; binding tightly to hydrophobic/aromatic sequences, and less tightly to hydrophilic sequences. We expect that the thermodynamic stability provided by tight binding will have different results for sequences in isolation versus those preceding folded domains. We predict that a tight interaction will slow peptide translocation, but increase the translocation rate of folded domains. Our results demonstrate that the ϕ clamp does bind to peptide probes, in a sequence- and driving-force dependent manner. We show that hydrophobic/aromatic sequences bind tightly to the channel, and are slow to translocate in isolation, but increase translocation rates when preceding a folded domain. Taken together, our data support the hydrophobic/steric ratchet mechanism of ϕ-clamp catalysis.

2.2 Results

Equilibrium ϕ-clamp affinity for peptide probes. Previous studies had identified the ϕ clamp as a binding site for hydrophobic/aromatic cations, we wanted to extend this analysis to amino acids (Krantz et al., 2005). We designed a series of 10-residue peptide probes, with host-

guest pattern (Figure 2.1A). Each probe has a conserved pattern of residues, 5 N-terminal lysines to ensure directional entry into the channel, and the remaining 5 residues contain the guest sequences of interest in a XXSXX pattern. We identify the peptides by the guest residue, e.g. Thr peptide has the sequence KKKKKTTSTT. We prepared representative probes for each category of amino acid, except charged residues. We kept the total charge constant for all peptides because we wished to avoid intermingling the study of hydrophobic/steric ratcheting with any possible effects of charge-state ratcheting.

We used planar lipid bilayer electrophysiology to measure equilibrium changes in ensemble WT PA current that corresponded to addition of peptide. Our experiments were done with a membrane potential ($\Delta\Psi$) of +20 mV as a driving force. As the concentration of peptide in the experiment is increased, the fraction of PA channels that are blocked increases, which indicates binding (Figure 2.1B). We plotted the fraction of current remaining against concentration of peptide and fit our data to a single binding site equation,

$$[I = I_o/(1 + K_{block}/[L]) + c] \quad \text{(Equation 2.1)}$$

to obtain K_{block} values (Figure 2.1C). In this equation I is the current amplitude, [L] is the peptide concentration, and c is an offset. Trp data were best fit with a cooperative, allosteric binding site model,

$$[I=I_0/(1+[L]/K1+([L]^2)/(K1*K2))+I_1*([L]/K1)/(1+[L]/K1+([L]^2)/(K1*K2))+I_2*(([L]^2)/(K1*K2))/(1 + [L]/K1 + ([L]^2/(K1*K2))] \quad \text{(Equation 2.2)}$$

where the first binding event does not block the channel, but does increase the affinity at the channel blocking (ϕ-clamp) site. In this equation K1 and K2 are the two equilibrium K_{block} values, [L] is the peptide concentration, I_1 and I_2 are the fractional current values corresponding to the first and second binding events, I_0 is the initial fractional current value and I is the final current amplitude. We found that K_{block} did depend on peptide sequence, with a positive correlation between binding affinity and probe hydrophobic surface area (Figure 2.2).

Force dependence of peptide K_{block}. We extended our equilibrium binding analysis to consider the force dependence of each peptide probe's K_{block}. We performed a series of identical electrophysiology experiments to those described above, but each experiment was conducted at a different $\Delta\Psi$. We measured K_{block} for each peptide under a wide range of driving forces, -5 mV to +70 mV. Trp peptide displayed consistent, cooperative, two binding-site behavior over this voltage range.

All peptide log K_{block} values exhibited nonlinear, or biphasic, $\Delta\Psi$ dependence (Figure 2.3A). Starting at -5 mV, we found that peptide binding affinity increased with increasing driving force. We observed the tightest binding around +40 mV, with little increase in affinity upon further increase in $\Delta\Psi$. We found that both Trp K_{block} values displayed biphasic voltage dependence, although our confidence in the value of K1, the non-occluding K_{block}, is low (Figure 2.3B). The overall trends in K_{block} that we observed at +20 mV were consistent across the $\Delta\Psi$ range, with hydrophobic/aromatic sequences displaying the tightest binding regardless of driving force.

Single channel analysis of peptide binding and translocation kinetics. Our previous measurements of peptide K_{block} were conducted at equilibrium, on an ensemble of thousands of PA channels. After establishing that the ϕ clamp does display sequence specific binding, we wanted to determine whether the interaction had any effect on peptide transport. By definition the equilibrium constant K_{block} is a ratio of the dissociation rate constants (k_{-1}+k_2; k_{unbind}+k_{trans}) and the association rate constant (k_1, k_{bind}) (Figure 2.4). If we conducted our electrophysiology experiments on a single PA channel we would be able to distinguish between

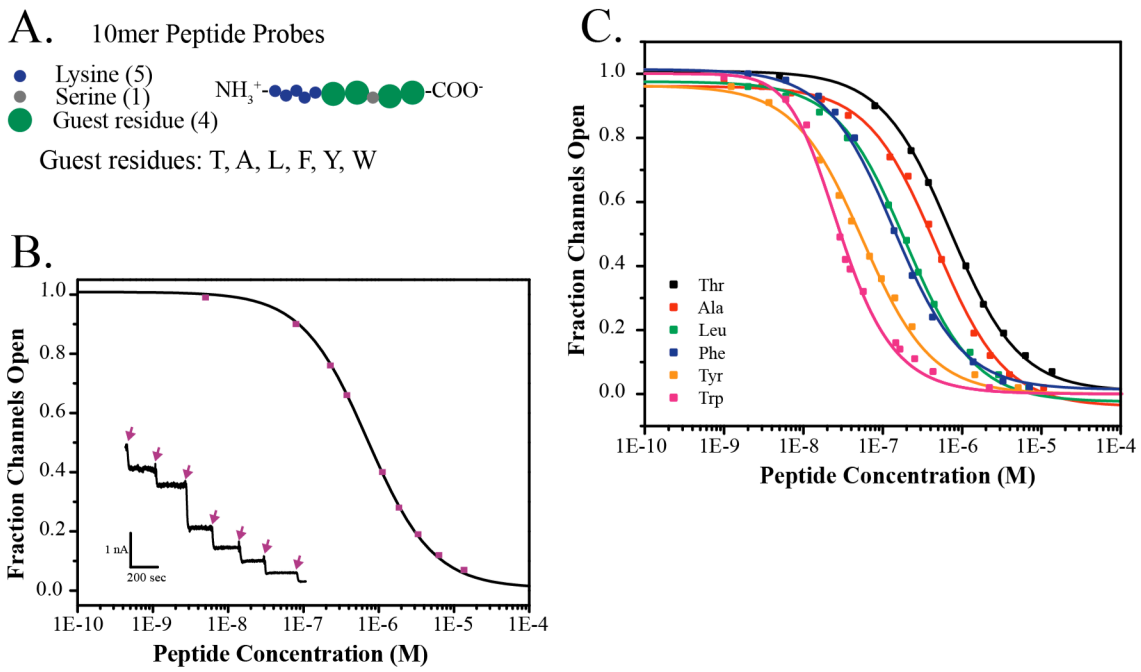

Figure 2.1. Peptide probes bind PA channels. (A) Diagram depicting our synthetic peptide probes. The peptides have a conserved pattern and are identified by the guest residue, e.g. Thr peptide has the sequence KKKKKTTSTT. **(B)** Example binding curve with fit line. The inset shows the titration data, in which the current decreases with every addition of peptide, as indicated by the arrows. The large graph shows the same data plotted as the fraction of open channels versus the concentration of peptide in the experiment. This dataset was collected with Thr peptide at +20 mV and symmetric pH 5.60. We fit each dataset with a single binding site model (Equation 2.1). **(C)** Binding curves for all peptides at +20 mV. Tryptophan peptide data fits best to a cooperative two-binding site model (Equation 2.2). These data illustrate the differences we observe in peptide binding affinity as we vary the guest residues in the peptides.

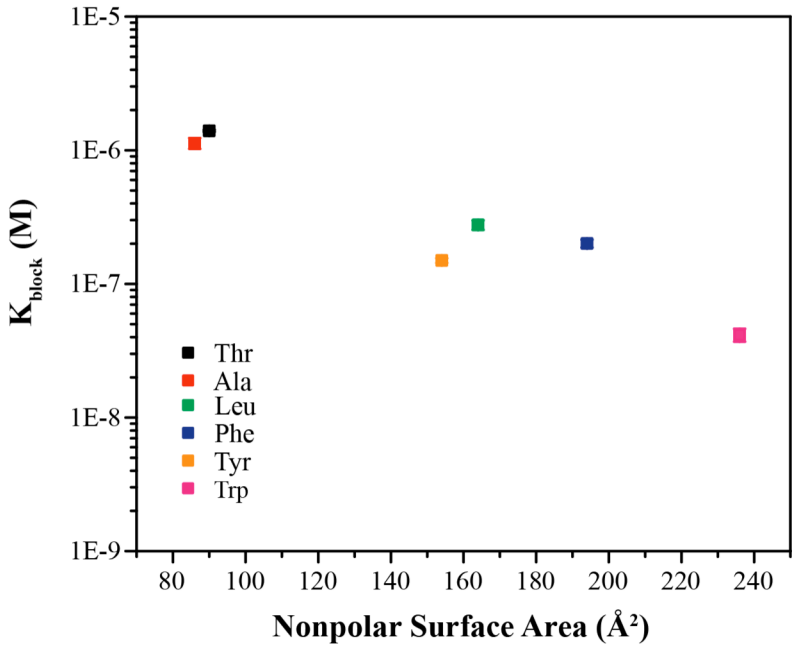

Figure 2.2. Peptide K_{block} correlates with nonpolar surface area. K_{block} values for each peptide probe collected at +20 mV and symmetric pH 5.60. The strength of the binding interaction at the ϕ clamp is positively correlated with the hydrophobic surface area of the probe. Error bars for all peptides are smaller than the data point. For clarity, only K2, the Trp K_{block} value corresponding to binding at the ϕ clamp, is displayed.

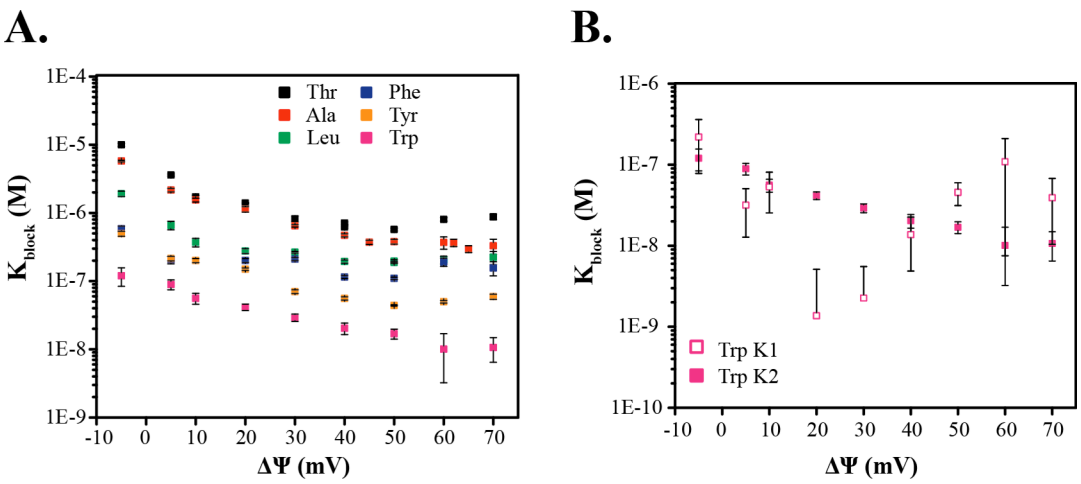

Figure 2.3. Biphasic force dependence of peptide K_{block}. (A) We measured peptide K_{block} values over a wide range of driving force, from -5 to + 70 mV, all at symmetric pH 5.60. The peptides with the greatest nonpolar surface area bound tightly to the ϕ-clamp across this entire range. Here we are only displaying K2, the Trp K_{block} that corresponds to channel blocking at the ϕ clamp. **(B)** Both Trp K_{block} values show biphasic voltage dependence, though K1, which corresponds to binding at the allosteric site, is measured with reduced accuracy. Error bars that are not visible are smaller than the data point.

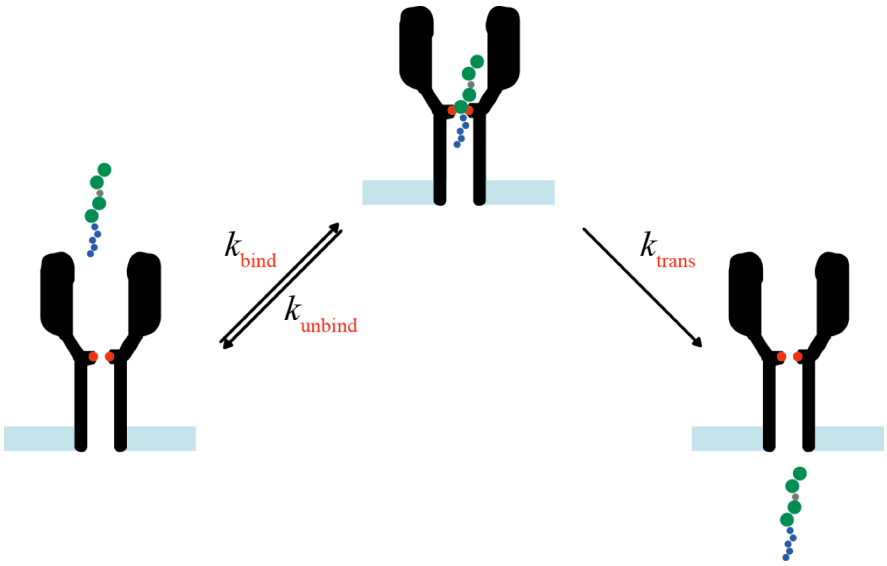

Figure 2.4. The equilibrium constant K_{block} is composed of three microscopic rate constants. The equilibrium constant we measured at steady state in our binding experiments has 3 contributing rate constants, such that $K_{block} = (k_{unbind}+k_{trans})/k_{bind}$. The association constant, k_{bind}, describes the binding reaction between the peptide and the ϕ-clamp. The dissociation of a bound peptide-clamp complex can happen in two ways. The peptide can unbind and exit the channel on the same side of the membrane it entered on, or the peptide can translocate through the channel and exit on the other side of the membrane. Thus the total dissociation constant has two components, k_{unbind} and k_{trans}, which have opposite force dependencies (Equation 2.4). We can measure each rate constant individually if we conduct experiments on a single PA channel, and we can use their different voltage dependencies to distinguish k_{unbind} from k_{trans}.

processes of association and dissociation and determine values for each rate constant. In the following kinetic experiments, we inserted one single PA channel into the membrane, added ~20 nM peptide, and recorded channel opening and closing activity as a function of $\Delta\Psi$.

We anticipated we would observe a two state system, where the channel had open (no peptide bound, full conductance) and bound (peptide bound at the ϕ clamp, no conductance) states. We believed the association constant k_{bind} would be simple to measure, as there is only one binding pathway, and we could identify binding events as a conducting channel losing conductance. However, there are two routes to unblock the channel. Closed-to-open transitions can occur for either productive translocation (k_{trans}) or unproductive retro-translocation (k_{unbind}); and therefore, $k_{obs} = k_{unbind} + k_{trans}$. We can deconvolute the two rate constants by obtaining the voltage dependence ($\Delta\Psi$) of the dissociation kinetics from +10 to +80 mV using Eyring-Woodhull analysis (Woodhull, 1973; Movileanu et al., 2005; Thoren et al., 2009). For a single-barrier model, the $\Delta\Psi$ dependence of $\Delta G^{\ddagger}$ should be linear,

$$\Delta G^{\ddagger}(\Delta\Psi) = \Delta G^{\ddagger}_{o} + zF\Delta\Psi \qquad \text{(Equation 2.3)}$$

where z is the charge dependence of the barrier crossing, F is Faraday's constant, and $\Delta G^{\ddagger}_{o}$ is the $\Delta G^{\ddagger}$ at 0 mV. For simple unimolecular processes this equation suffices. However, when there are two routes for a given process, such as peptide dissociation, then we rely on the unique $\Delta\Psi$ dependencies of the fundamental rate constants describing each route. For example, unproductive retrotranslocation has an oppositely-signed z-value from productive translocation, and hence the $\Delta\Psi$ dependence of $\Delta G^{\ddagger}$ for the dissociation kinetics is chevron-shaped,

$$\Delta G^{\ddagger}(\Delta\Psi) = RT\ln[\exp((\Delta G^{\ddagger}_{o1} + z_1F\Delta\Psi)/RT) + \exp((\Delta G^{\ddagger}_{o2} + z_2F\Delta\Psi)/RT)] \qquad \text{(Equation 2.4)}$$

We expected the total dissociation constant to have this biphasic force-dependence plot, with the low $\Delta\Psi$ arm predominantly due to k_{unbind} (which decreases with increasing $\Delta\Psi$) and the high $\Delta\Psi$ arm predominantly due to k_{trans} (which increases with increasing $\Delta\Psi$).

We were able to identify the expected open and bound states as well as two additional, partially conducting states, that represented interactions with peptide probes (Figure 2.5). We found that the additional states, which we are calling I_1 and I_2, depend on both peptide sequence and $\Delta\Psi$. I will discuss the intermediate states in great detail in Chapter 3. For the following kinetic analysis, we ignored the two intermediate states and focused only on transitions directly between open and bound states. We plotted peptide dwell times at each state as cumulative distribution functions (CDF) and then fit our data to single exponentials,

$$[y = y_0 - \exp(-\lambda * x)] \qquad \text{(Equation 2.5)}$$

to determine rate constants, shown here as λ, for each process (Figure 2.6).

We found that peptide binding rates were concentration and $\Delta\Psi$ dependent, as we expected for an association process (Figure 2.7A). As the peptide concentration or $\Delta\Psi$ is increased, peptide k_{bind} values increase. The accuracy in measuring k_{bind} is limited by our equipment at high $\Delta\Psi$, so we report k_{bind} for all peptides at +20 mV (Figure 2.7B). We found a slight positive correlation between nonpolar surface area and peptide k_{bind}, with larger probes binding more quickly, although the overall differences in rate are small. The Tyr k_{bind}, which is much greater than the other probes, is likely to be overestimated due to side chain absorbance complicating the backbone absorbance assay we used to determine concentration.

Peptide dissociation rates were concentration independent, as we expected because we were measuring the decay of a single complex (Figure 2.7C). The overall force dependence of dissociation was chevron shaped, which confirmed our original analysis of the rate constants that comprise K_{block} (Figure 2.7D). We found that peptide rates were consistent across the $\Delta\Psi$ range;

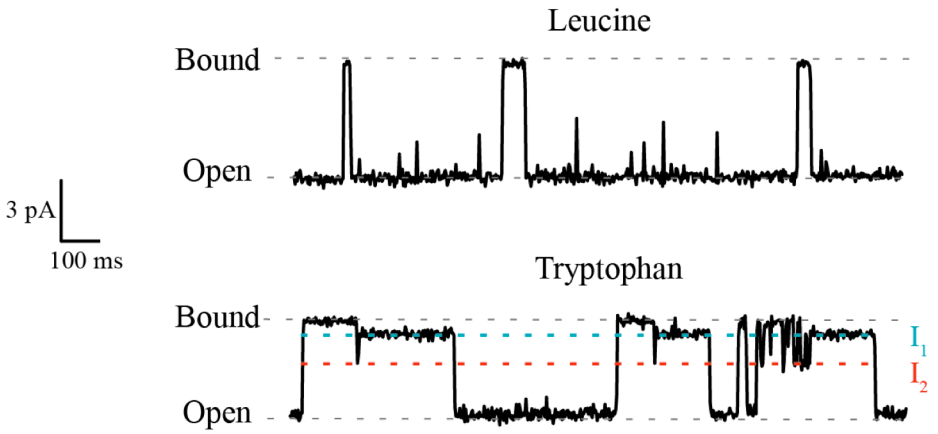

Figure 2.5. Single channel electrophysiology reveals kinetics of peptide binding to the ϕ clamp. The top trace shows a single channel WT PA interacting with Leu peptide at +70 mV and pH 5.60. Along with Thr and Ala, Leu predominantly exhibited simple bound and unbound states. The bottom trace shows a Trp peptide interacting with a single WT PA channel at +70 mV and pH 5.60. Trp, Tyr, and Phe peptides all displayed kinetic intermediate conductance states (I_1 shown in blue and I_2 shown in red), in addition to bound and open states. We are ignoring the intermediates for this kinetic analysis, and focusing only on transitions between open and bound states. We can measure the time the peptide dwells in each state as a function of driving force to determine each of the 3 microscopic rate constants.

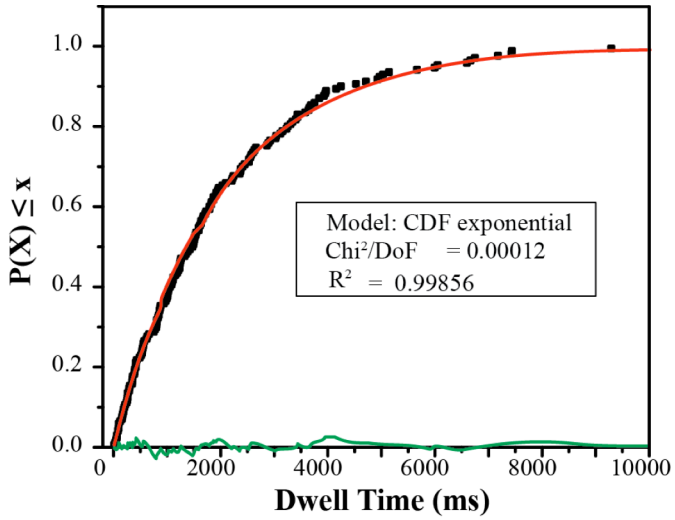

Figure 2.6. Single channel peptide kinetic data are fit as cumulative distribution functions (CDFs). This example shows a complete dataset for Thr peptide binding transitions at +40 mV. We extract dwell times from raw electrophysiology data, plot them as a CDF, and fit with a single exponential equation (Equation 2.5). Each black point represents an individual dwell time that we measured. The CDF fit, in red, and the residual, in green, are included to illustrate that our data fit nicely to a single exponential function. All binding datasets fit to single exponentials. Translocation datasets for Thr, Ala, and Leu fit to single exponentials, but those for Trp, Tyr, and Phe are often best fit by double exponentials, which indicates the presence of kinetic intermediates in the bound to open transitions.

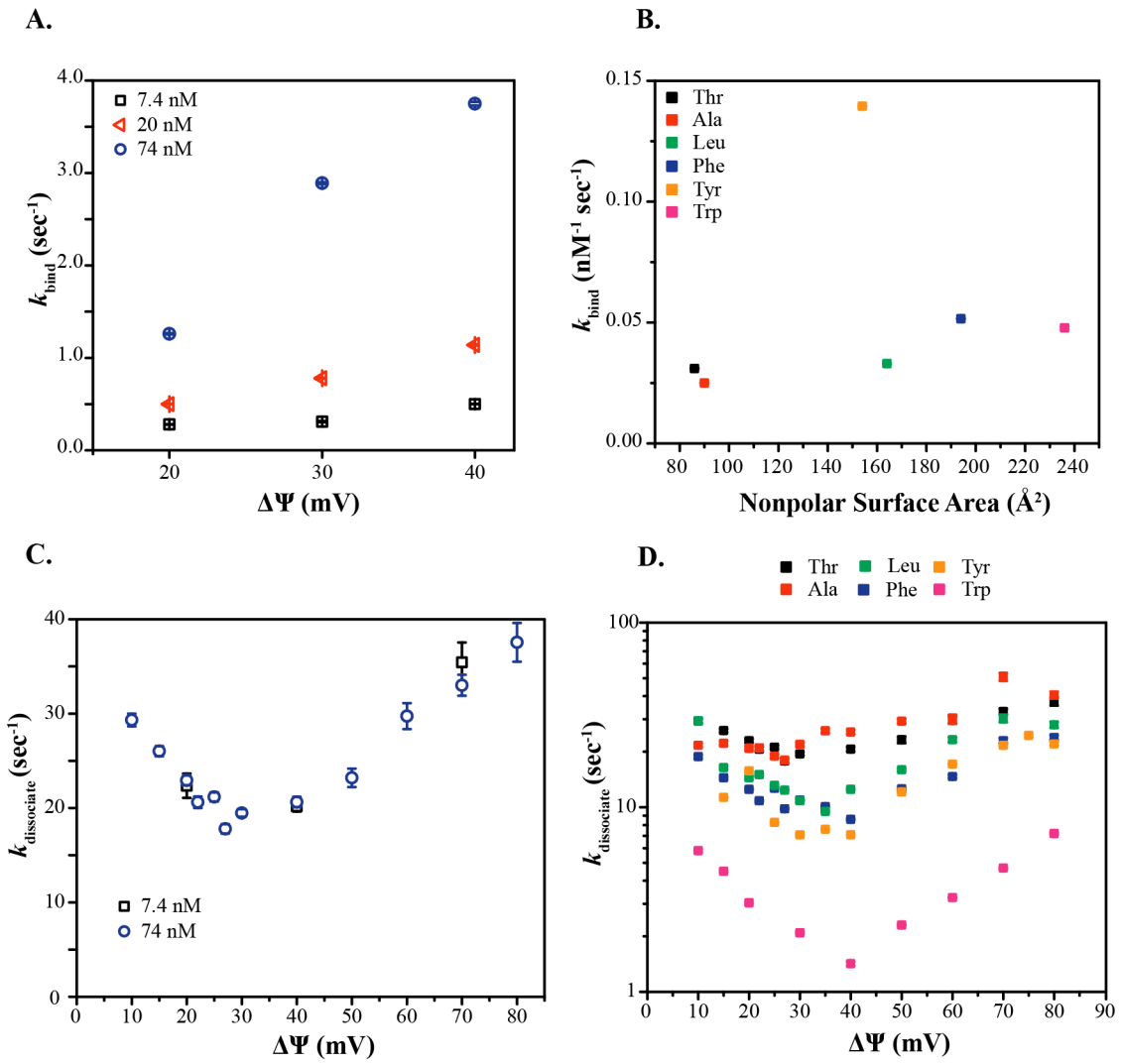

Figure 2.7. Rate constants for peptide binding and dissociation processes vary with sequence and driving force. **(A)** Peptide binding rates increase as a function of voltage and concentration. Thr peptide is shown here as an example. **(B)** Binding rates correlate positively with nonpolar surface area. These rates are for all peptides at +20 mV. Generally, more hydrophobic sequences bind more quickly to the channel, although the rate difference between the slowest and fastest constants is not large. **(C)** Peptide dissociation rates have a biphasic dependence on voltage and are concentration independent. Thr peptide is shown as an example. The arm with the negative slope (low ΔΨ) corresponds to k_{unbind}, which should decrease as we increase the force, and the arm with the positive slope (high ΔΨ) corresponds to k_{trans}, which should increase as we increase the force. **(D)** Dissociation constants for all peptides have chevron-shaped voltage dependence. Hydrophobic/aromatic peptides are slow to unbind and slow to translocate. Our kinetic data reinforce the results of our equilibrium data; large hydrophobic/aromatic sequences that bind tightly to the channel are slow to be released. Any error bars not visible in this figure are smaller than the data point.

probes slow to unbind at low ΔΨ were slow to translocate at high ΔΨ. Overall the slowest peptides were hydrophobic/aromatic, the fastest were small/polar (Figure 2.7D).

Kinetic analysis of probe interactions with ϕ-clamp mutants. We wanted to confirm that our equilibrium and kinetic results were due to a specific interaction between the ϕ clamp and our probes, as opposed to a nonspecific interaction elsewhere in the channel. The WT clamp is composed of phenylalanine residues; here we used tyrosine and alanine mutants. F427Y mutants have reduced translocation kinetics and F427A mutants can not translocate protein at all. (Krantz et al., 2005) Small molecules cannot bind to mutant ϕ clamps but we predicted that given their larger size, our peptides would retain binding ability. We hypothesized that if the peptides were specifically interacting with the ϕ clamp, mutant clamps would alter peptide transportation kinetics, and if the peptides were interacting elsewhere in the channel we would see no effect.

We conducted single channel kinetic experiments at +70 mV, as described previously. At this ΔΨ we expected to be well into the regime where k_{trans} is the predominant factor in the dissociation constant. We collected data with our probes and the mutant PAs and then normalized the rate constants to those we measured with WT PA. Both ϕ-clamp mutants we tested showed altered translocation kinetics for all the probes (Figure 2.8). We found that non-aromatic peptides were transported more slowly by the mutant clamps; aromatic peptides were transported more quickly by the mutants. Tyr peptide showed both trends; translocation was slow with F427A but fast with F427Y. These experiments confirmed that all of our electrophysiology data were a consequence of a direct interaction between the ϕ clamp and the probes.

Bulk translocations of model multi-domain substrates. After we established how specific peptide sequences were transported by PA, we wanted to know how these same sequences affected translocation of a folded protein. We hypothesized that when the ϕ clamp was presented with a hydrophobic/aromatic sequence preceding a folded domain, it would act as a hydrophobic/steric ratchet. A tight interaction with the ϕ clamp could lower the unfolding barrier for the rest of the protein, and once the interacting region of the substrate translocated through the ϕ clamp it would be sterically blocked from retrotranslocating. Ultimately, we predicted that hydrophobic/aromatic sequences would result in faster transport of folded domains. To test this hypothesis we designed a series of model substrates consisting of the LF binding domain (LF_N) with a synthetic 25 residue C-terminal linker to Diphtheria Toxin A chain (DTA) (Figure 2.9A). We chose to use LF_N to provide specific binding to PA. The synthetic linker region between LF_N and DTA has a random Gly-Ser-Thr backbone that we modified with our residues of interest, in two different patterns. The constructs are identified by the one-letter code for the guest amino acid and the notation d (for dense) or s (for sparse), which indicates the relative spacing of guest residues in the linker, e.g. LF_N-Td-DTA contains a densely pattern Thr guest sequence. The parent construct, which is the control for the sparse sequences, is identified as LF_N-GST-DTA.

We used ensemble planar lipid bilayer electrophysiology to monitor translocation, similar to how we monitored peptide binding. In our translocation experiments, thousands of PA channels are inserted into an artificial lipid bilayer. Substrate is added to the bilayer at ~20 nM and as it binds to PA it blocks conductance. Perfusion removes excess substrate, and translocation is initiated by increasing the ΔΨ. As the substrate translocates, the channel becomes unblocked, and the restoration of conductance reports on the translocation kinetics in real time. From the translocation half time ($t_{1/2}$), which is the time (measured in seconds) for half

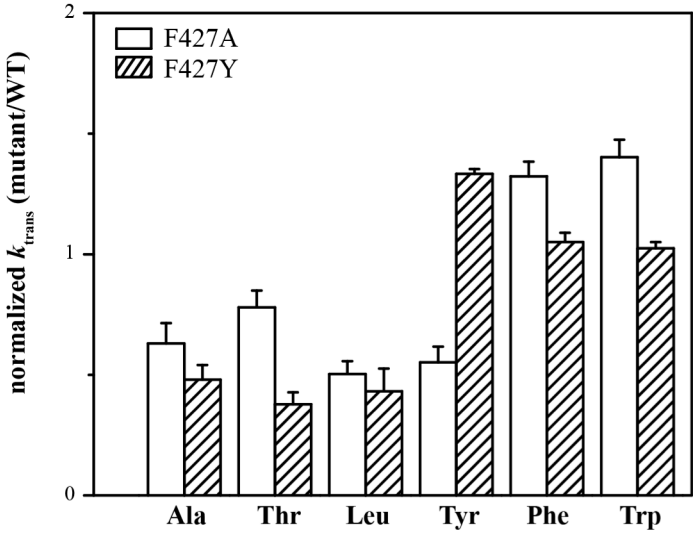

Figure 2.8. ϕ-clamp mutations alter peptide translocation kinetics. We measured translocation kinetics at +70 mV and symmetric pH 5.60 for our peptides with two ϕ-clamp mutants, F427A and F427Y, which have been previously shown to have translocation defects. We then normalized these results to the values obtained for WT PA. Both ϕ-clamp mutants showed altered transport of all peptides, demonstrating that the peptides are interacting with the ϕ clamp. The transport of aromatic hydrophobic residues was not inhibited by either PA mutant, however transport of small or hydrophilic residues was slowed. Tyr peptide, which is aromatic but not particularly hydrophobic, was transported more slowly by F427A but more quickly by F427Y, relative to WT. Leu, which is hydrophobic, was transported more slowly by both mutants. Thus, aromaticity is likely the most important determinant in ϕ-clamp interactions. Our results indicate that the transport of Trp and Phe peptides is limited by a steric clash at the site of the ϕ clamp, as mutations that shrink the size of the clamp increase translocation rate relative to WT.

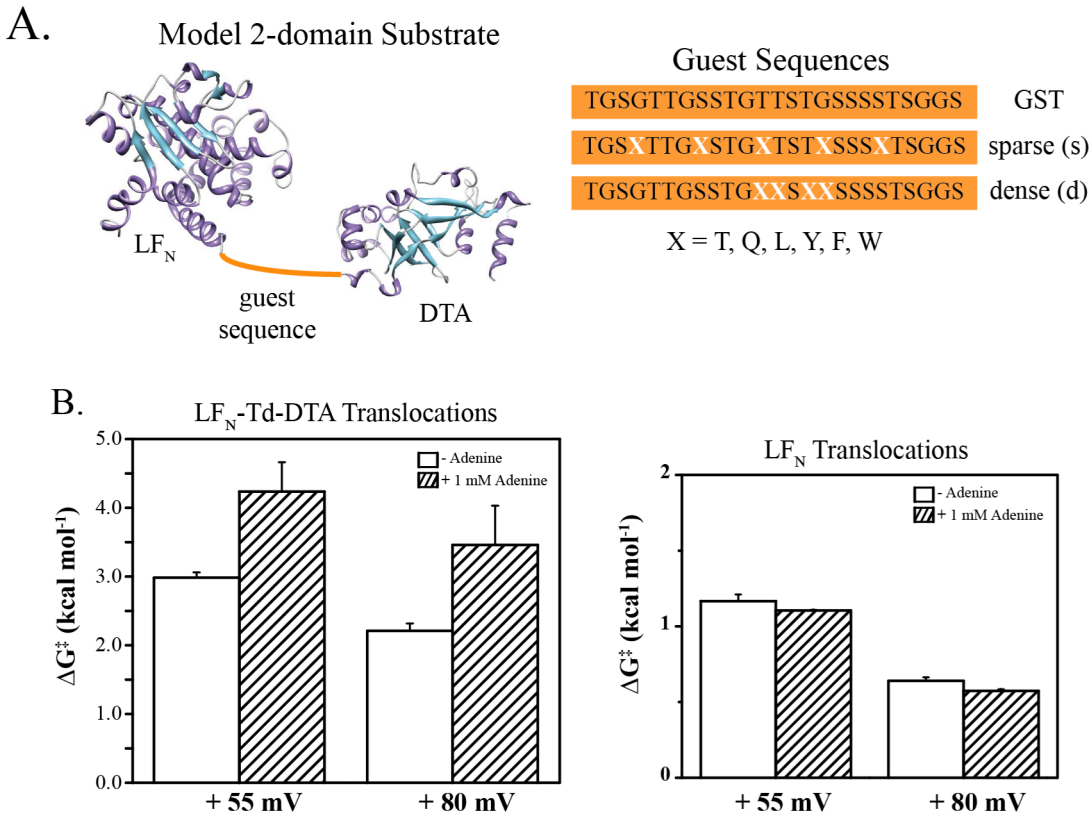

Figure 2.9. Translocation of second domain in model substrates is rate limiting. **(A)** Design of the multi-domain substrate construct. LF_N, the binding domain of LF, a natural PA substrate, is linked to Diphtheria Toxin A chain (DTA) via a 25 residue guest region. Within this variable test region we add residues of interest, in one of two patterns. The constructs are identified by the 1 letter code for the guest amino acid, followed by s (sparse) or d (dense), which indicates the relative spacing of the guest residues within the linker; e.g. LF_N-Td-DTA contains a densely patterned Thr guest sequence. The control construct for the sparsely patterned residues is a random sequence of Gly, Ser, and Thr residues that is identified as LF_N-GST-DTA. The GST sequence serves as the backbone for all the test sequences. **(B)** Translocation of LF_N-Td-DTA is impeded by DTA stabilization. We assayed translocation by bulk electrophysiology at symmetric pH 5.60, and used $t_{1/2}$, the time for half of the protein to translocate, to calculate an activation energy ($\Delta G^{\ddagger} = RT \ln t_{1/2} / c$). R is the gas constant, T is temperature, and c is a 1-second reference constant. Addition of 1 mM adenine, which specifically stabilizes DTA, slowed translocation of LF_N-Td-DTA but not LF_N alone. This indicates that under our experimental conditions, the PA mediated unfolding and translocation of DTA is rate limiting. Error bars not visible in this figure are smaller than the data points.

of the translocated protein to move through the channel, we can calculate an empirical activation energy ($\Delta G^{\ddagger}$) at a particular $\Delta\Psi$, where $\Delta G^{\ddagger} = RT \ln t_{1/2} / c$. R and T are the gas constant and temperature, respectively, and c is an arbitrary reference, which we define as 1 s. We can also measure the fraction of protein that is translocated. Translocation efficiency (ε) is defined by $\varepsilon = A_{obs}/A_{exp}$, where A_{obs} is the observed amplitude of channels that reopened in the course of the experiment, and A_{exp} is the expected amplitude if all of the channels reopened.

In order for our sequences to have any effect on translocation kinetics, the PA catalyzed unfolding and translocation of DTA must be rate limiting for the transport of the model substrates. We compared translocations of LF_N-Td-DTA in the presence and absence of adenine, which is a substitute for NAD^+, the natural cofactor of DTA (Wesche et al., 1998; Zhang et al., 2004). Addition of 1 mM adenine greatly slowed translocation and reduced LF_N-Td-DTA ε at both voltages we tested, but had no effect on LF_N alone (Figure 2.9B). These results confirmed that the unfolding and translocation of DTA was the rate-limiting step in our multi-domain translocations.

We then translocated our complement of multi-domain substrates across a range of voltages (Figure 2.10A). We found that the proteins containing aromatic guest sequences translocated the fastest across all $\Delta\Psi$, which we are reporting as lower $\Delta G^{\ddagger}$ values. Our preliminary results show that dense and sparse patterning within the guest region does affect kinetics, but we still observe the aromatic-residue rate enhancement with both types of substrates, with no effect on translocation efficiency (Figure 2.10B). The densely patterned Trp sequence provided a reduced rate enhancement relative to a sparsely patterned sequence, but we would need to compare more dense sequences to be sure that it isn't an effect of proximity to the folded domain, rather than pattern. We translocated LF_N-Wd-DTA in the presence of 1 mM adenine to determine whether the Trp residues could compensate for stabilized DTA. We found no difference in $\Delta\Delta G^{\ddagger}$ values for adenine stabilization of threonine and tryptophan sequences, and under these conditions, LF_N-Wd-DTA translocated equivalently to LF_N-Td-DTA (Figure 2.10C).

2.3 Discussion

Hydrophobic gaskets are a common motif in translocase channels; they provide important interaction sites for substrates and can play roles in energy transduction. Here we investigated the activity of the ϕ clamp, the hydrophobic gasket from the PA channel. The ϕ clamp is known to contact substrates and catalyze unfolding and translocation, though the mechanism is not fully understood. The results presented here support the hypothesis that the ϕ clamp acts as a hydrophobic/steric ratchet to unfold and translocate proteins. We show that the ϕ clamp binds tightly to hydrophobic/aromatic sequences, and that this interaction slows transport of peptides, but increases transport rates of folded proteins. We propose a model in which the substrate/ϕ-clamp interaction reduces the barrier for substrate unfolding while simultaneously preventing counterproductive retrograde movement of the polypeptide chain.

Hydrophobic/aromatic sequences bind the ϕ clamp. We used a series of 10-residue peptides with a host-guest pattern to demonstrate that different sequences bind the channel with different affinities (Figure 2.2). Previous studies had identified the ϕ clamp as a hydrophobic/aromatic cation binding site, our results extend this to include hydrophobic/aromatic amino acids (Krantz et al., 2005). We used single channel analysis of ϕ clamp mutants to confirm that our probes were binding at the ϕ clamp (Figure 2.8).

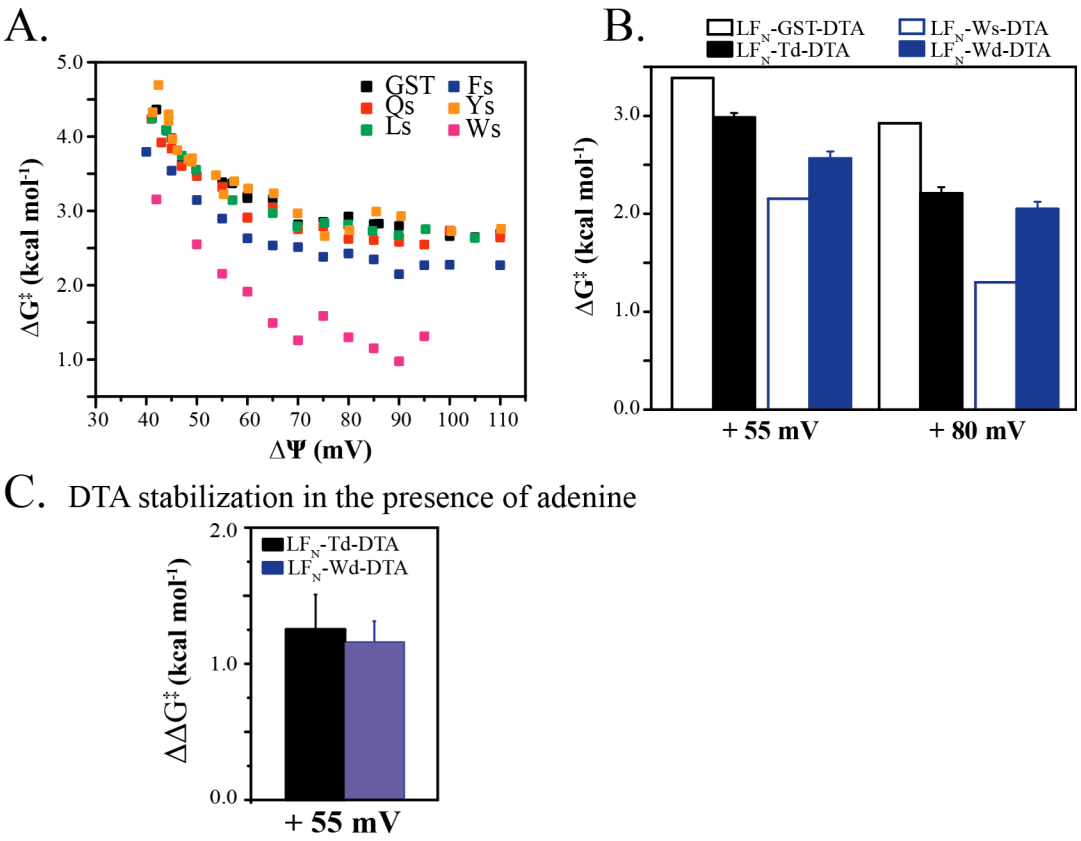

Figure 2.10. Hydrophobic/aromatic sequences increase translocation of multi-domain substrates by modulating protein stability. (A) Force dependence plot of all sparse construct translocations, measured at symmetric pH 5.60 with WT PA. Lower $\Delta G^{\ddagger}$ values reflect faster translocation. The constructs containing the most hydrophobic/aromatic sequences were transported the fastest. **(B)** Guest residue patterning affects translocation. Comparing translocation rates of densely patterned vs sparsely patterned sequences showed tryptophan containing linkers with sparse patterning were transported more quickly. All constructs were translocated with similar efficiency. **(C)** Addition of 1 mM adenine resulted in similar $\Delta\Delta G^{\ddagger}$ values for LF_N-Wd-DTA and LF_N-Td-DTA translocation, where $\Delta\Delta G^{\ddagger} = \Delta G^{\ddagger}_{adenine} - \Delta G^{\ddagger}_{control}$, thus adenine stabilized the constructs equally. The adenine-based stabilization of DTA eliminates the tryptophan sequence-dependent rate enhancement.

We found that the strength of the interaction at the ϕ clamp scaled with the peptide's nonpolar surface area, which indicates that we were measuring a hydrophobic interaction. Tryptophan residues, which are both bulky and hydrophobic, interacted most tightly with the ϕ-clamp under all the conditions we tested. We were not surprised by these results; the ϕ-clamp itself is quite hydrophobic, and the ordering of water around hydrophobic residues is entropically unfavorable, so it makes sense for the hydrophobic clamp to interact with similarly nonpolar residues.

Tryptophan sequences bind a second site in the channel. The equilibrium binding data we collected with Trp peptide fit best to a cooperative allosteric binding site model, rather than the simple single binding site model that fit the other peptide data (Equations 2.1 and 2.2). The Trp data suggest that there are 2 binding sites, one allosteric site that doesn't interfere with conductance, and a second site that does block the channel. Affinity at the channel-blocking site, the ϕ clamp, is increased by binding events at the first site. We speculate that the allosteric site could be the α clamp, which we know binds tryptophan-containing sequences. A binding event at this site would not block conductance at the ϕ clamp (Feld et al., 2010). To test this hypothesis we plan to measure Trp binding to a PA mutant with a defective α clamp, such as PA R178A (Feld et al., 2010). If PA R178A Trp binding data fit to a single binding site model we can be sure the allosteric binding site is the α clamp. We also plan to measure Trp binding to ϕ-clamp mutants, which should provide a greater separation between the two K_{block} values and allow us to measure K1 more accurately.

Hydrophobic/aromatic sequences translocate slowly in isolation. We used single channel electrophysiology dwell time analysis to measure the three microscopic rate constants that comprise the equilibrium constant K_{block} (Figure 2.4). We were able to identify the peptide binding rate constant due to its dependence on substrate concentration and force (Figure 2.7A). We used Eyring-Woodhull analysis to distinguish the rate constants for the two types of dissociation processes (Figure 2.7D, Equation 2.4). Based on our analysis, we conclude that the low ΔΨ regime is related to unbinding, or peptides being released to the pool of free peptide; the high ΔΨ regime is related to translocation, or peptides being released to the other side of the membrane.

The binding rate constants we measured correlated positively with nonpolar surface area, the fastest binders were the largest most hydrophobic peptides (Figure 2.7B). The Tyr binding rate constant was 3-fold faster than any of the other constants, which may be due to complications in determining the peptide concentration. We plan to confirm the concentration and normalize the data to reflect the accurate value.

We found a different trend for dissociation rates; the largest hydrophobic/aromatic peptides had the slowest unbinding (low ΔΨ) and translocation (high ΔΨ) rate constants (Figure 2.7D). This was true across the entire driving force range we tested. Our kinetic results recapitulated the equilibrium K_{block} trends we saw previously; tight binding is a product of fast association and slow dissociation, and supported our hypothesis that a tight interaction between a probe and the ϕ-clamp would result in slow translocation.

We used mutant ϕ clamps to address the steric effects of the clamp-sequence interaction. The bulkiest residues, Trp and Phe, were transported more quickly by mutant clamps; the smallest residues were translocated more slowly by the mutants (Figure 2.8). Tyr, which is large but more hydrophilic, was transported slowly by F427A and more quickly by F427Y. Leu transport was slowed by both mutants, which indicates that aromaticity is probably the more important determinant in the sequence-specific interaction with the ϕ clamp. The bulky nature of

aromatic residues is likely to be responsible for their slow translocation, as steric clashes with the ϕ clamp could occur as they move through the channel, slowing transport. By virtue of their bulk, these residues are often quite hydrophobic, so it is difficult to fully isolate each factor. We find it likely that there is a trade-off between efficient transportation of large residues and small residues, and we propose that the ϕ clamp and other hydrophobic gaskets have been optimized to work efficiently on all side chain chemistries.

Hydrophobic/aromatic sequences increase translocation rates of folded domains. Hydrophobic/aromatic residues are often found in the core of folded proteins, and burial of hydrophobic residues is a major driving force for protein folding. Proteins generally have hydrophobic residues, and many proteins are unfolded and moved across membranes. Given all this, why would protein transport channels have evolved structures that interact tightly with hydrophobic residues, if the interaction slows translocation? Based on our hydrophobic/steric ratchet hypothesis we predicted that the translocation rate of a folded domain would actually be increased by upstream hydrophobic residues. We expected this to be primarily a result of the ϕ clamp binding exposed hydrophobic residues and stabilizing partially unfolded substrates, leading to an overall increase in unfolding rates. We predicted that once bulky sequences had passed through the ϕ clamp, they would be slow to pass back through due to steric exclusion, which would bias motion in the translocation direction and could prevent backsliding if the driving force momentarily subsided.

We used a series of two-domain substrates to determine how different residues in the linker region between the domains affected translocation of the C-terminal domain. We stabilized the downstream domain and observed a decrease in translocation rate, which confirmed that transport of this domain was rate limiting (Figure 2.9B). We found that hydrophobic/aromatic residues in the linker region decreased the $t_{1/2}$ of the downstream domain without reducing the amount of protein that was translocated (Figure 2.10A). In these experiments, Trp and Phe showed the greatest rate enhancements while Tyr showed a minimal rate enhancement. These results suggest that aromaticity alone is not enough, and that the hydrophobic nature of the substrate is also important.

We observed that stabilization of the downstream domain abrogated the tryptophan based rate enhancement, which further supports our conclusion that the bulky hydrophobic/aromatic sequences act at the level of protein stability (Figure 2.10C). We found that the spacing of the residues is important for the effect, and our preliminary data indicate that a densely patterned sequence provides a smaller rate enhancement than a sparsely patterned sequence (Figure 2.10C). We believe this effect could be due to proximity of the residues to the folded domain rather than to the pattern itself, and plan to test other spacing patterns to verify this hypothesis.

PA uses a hydrophobic/steric ratchet to drive unfolding and translocation. Our results are consistent with a ratchet driven mechanism of PA translocation. Previous work has shown that PA can use a substrate based charge-state ratchet to drive unfolding and bias Brownian motion (Brown et al., 2011). In this work we provide evidence that PA can also function as a hydrophobic/steric ratchet; the ϕ clamp serves as a pawl in the ratchet, binding tightly to hydrophobic/aromatic sequences in the substrate (Figure 2.11). It is likely that the steric bulk of the substrate sequence is more important than pure hydrophobicity for this mechanism, hence the name hydrophobic/steric ratchet. The steric bulk of the ϕ clamp allows it to bias thermal motion by acting as a “one-way door"; retrotranslocation of bulky sequences through the clamp would be very slow. Thus the clamp acts as a pawl in a ratchet, biasing motion of the polypeptide by preventing backsliding. This would be especially useful should the

driving force temporarily subside. Substrate engagement at the ϕ clamp simultaneously increases the unfolding and subsequent translocation of the substrate by lowering the barrier for unfolding. The hydrophobic/steric ratchet concept I have described is applicable to any translocase system in which a hydrophobic clamp structure makes contact with the substrate. We believe that the hydrophobic gaskets of other protein transport machines, such as the AAA+ family of unfoldase/translocases, could act as hydrophobic ratchets without compromising their function in power stroke force transduction.

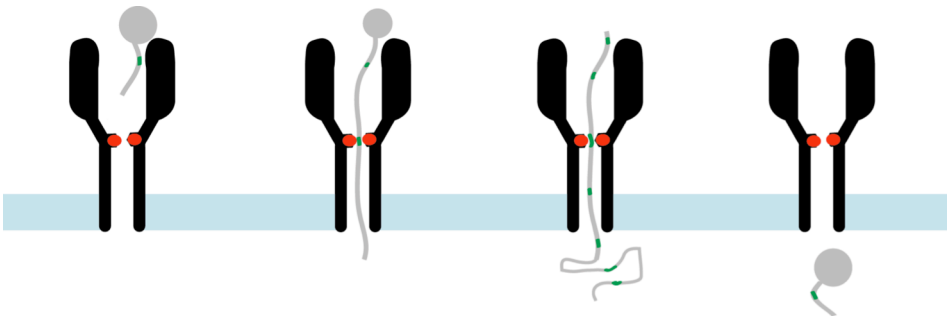

Figure 2.11. PA's ϕ clamp acts as a hydrophobic/steric ratchet to drive unfolding and translocation. We propose a model in which the ϕ clamp, shown in red, interacts favorably with hydrophobic/aromatic sequences, shown in green, that are exposed as the substrate unfolds. This interaction has several important consequences. The ϕ clamp provides a hydrophobic interaction surface that reduces the energetic penalty for exposing hydrophobic residues in the substrate to the aqueous environment. This would effectively lower the barrier for further substrate unfolding. After a sequence passes through the ϕ clamp, the clamp provides a steric hindrance to prevent backsliding and direct motion productively. Ultimately the ϕ clamp catalyzes protein unfolding and translocation via processive interactions with exposed hydrophobic/aromatic sequences in the translocating chain.

2.4 Materials and methods

Peptides. All short oligopeptides were synthesized and purified to >95% (Elim Biopharmaceuticals, Hayward, CA). Peptides were dissolved in ultra pure H_2O and concentrations were determined using backbone and/or residue absorbance, when the sequence contained Tyr or Trp residues.

Proteins. WT and PA mutants were expressed, purified, and oligomerized as previously described (Thoren et al., 2009). His_6-LF_N-guest-sequence-DTA expression system was constructed from residues 1-263 of LF followed by the A chain of diphtheria toxin (DTA) sequence contained in a pET15b expression vector (Krantz et al., 2005). A Not I site located after the C terminus of LF_N and a Spe I site followed by a thrombin recognition site just before the N terminus of DTA were engineered into the pET15b construct. These unique restriction sites allowed insertion of synthetic 25-residue guest sequence. Not I/Spe I-flanked DNA cassettes encoding the desired guest peptide sequences were synthesized and cloned according to previously described gene synthesis methods (Feld et al., 2010; Brown et al., 2011). His_6-LF_N-guest-DTA proteins were purified from overexpressing bacteria using standard Ni^{2+}-nitrilotriacetic acid affinity chromatography and Blue Sepharose affinity (BS) chromatography. Proteins containing extremely hydrophobic guest sequences were isolated from inclusion bodies and further purified by BS chromatography.

Electrophysiology. Planar lipid bilayer electrophysiology data were recorded using an Axopatch 200B amplifier (Molecular Devices Corp., Sunnyvale, CA) in voltage-clamp mode as described (Kintzer et al., 2009; Thoren et al., 2009). Membrane bilayers were painted onto a 100-μm aperture of a 1-ml delrin cup with 3% 1,2-diphytanoyl-sn-glycero-3-phosphocholine (Avanti Polar Lipids, Alabaster, AL) in neat *n*-decane. Cis (side to which the PA oligomer is added) and trans chambers were bathed in the indicated buffers as required. Experiments were conducted under a membrane potential, $\Delta\Psi \equiv \Psi_{cis} - \Psi_{trans}$ ($\Psi_{trans} \equiv 0$ V).

For ensemble peptide-binding electrophysiology, planar lipid bilayers were bathed in universal pH 5.60 bilayer buffer (UBB: 10 mM oxalic acid, 10 mM phosphoric acid, 10 mM MES, 1 mM EDTA). PA oligomers were added to the cis chamber under a $\Delta\Psi$ of +20 mV and allowed to form channels. When the total current in the experiment reached ~5000 pA excess PA was perfused away. The $\Delta\Psi$ was then adjusted in the range of -10 mV to +80 mV. Small aliquots of peptide were then added to the cis chamber and allowed to equilibrate. Binding of peptide to the channels resulted in blocking of the channel and a decrease in total current. The total concentration of peptide added and the fraction of channels still conducting were recorded until all channels were effectively blocked by peptide.

For single-channel peptide translocation, planar lipid bilayers were bathed in symmetric single channel buffer (SCB: 100 mM KCl, 1 mM EDTA, 10 mM succinic acid, pH 5.60). PA oligomer was applied directly to membranes at 10^{-16} M. Single channel insertion was observed by a discrete increase in current under an applied voltage of +20 mV. Once a single channel had inserted into the membrane, peptide was added to the cis side of the membrane at 18-20 nM. Data were recorded at 400 or 600 Hz using a low pass filter of 200 Hz under varying applied $\Delta\Psi$.

For ensemble LF_N-guest-peptide-DTA translocation assays, translocation experiments were carried out using UBB at symmetric pH 5.60 as described (Kintzer et al., 2009; Thoren et al., 2009). Where indicated adenine was added at 1 mM to UBB on both sides of the membrane. Membranes were formed and channels were inserted as described for bulk peptide binding experiments. His_6-LF_N-guest-peptide-DTA substrate was added to the cis-side of the membrane

at 20 nM, and binding was monitored as a decrease in current. Excess substrate was removed by perfusion and the translocation process was initiated by increasing the $\Delta\Psi$.

Data Analysis. We fit peptide titration data to a simple single-binding site model, $I = I_o/(1 + K_d/[L]) + c$, to obtain the equilibrium dissociation constant, K_{block}, where I_o is the current amplitude, [L] is the peptide concentration, and c is an offset. Trp data were fit to a cooperative allosteric binding site model [$I = I_0 / (1 + [L]/K1 + ([L]^2)/(K1*K2)) + I_1*([L]/K1)/(1 + [L]/K1 + ([L]^2)/(K1*K2)) + I_2*(([L]^2)/(K1*K2))/(1 + [L]/K1 + ([L]^2/(K1*K2))$]. In this equation K1 and K2 are the two equilibrium constants, [L] is the peptide concentration, I_1 and I_2 are the fractional current values corresponding to the first and second binding events, I_0 is the initial fractional current value and I is the final current value. We first analyzed all the Trp data to arrive at a set of parameter values, which we then fixed and analyzed again. For all the Trp datasets we fixed I_0 at 0.98, I_1 at 1, and I_2 at 0.0013.

For single channel kinetic analysis, dwell times were extracted from datasets using the single channel tool in CLAMPFIT10.2 (Molecular Devices, Sunnyvale, CA). We excluded short duration (<7 ms) dwell times due to our data collection filtering settings. Dwell times were compiled into cumulative distribution functions (CDF) in MATLAB (MathWorks, Natick, MA). Each CDF was fit with a single exponential function [$y = y_0 - \exp(-\lambda*x)$], in ORIGIN (OriginLab, Northampton, MA) to determine rate constants (λ) for each observed transition.

Protein translocation was quantified as the time for half the protein to translocate ($t_{1/2}$). We calculated translocation activation energies ($\Delta G^{\ddagger}$) for each translocation, where $\Delta G^{\ddagger} = RT \ln t_{1/2} + c$. R is the gas constant, T is the temperature, and c is the natural log of 1 second. We also report the change in $\Delta G\ddagger$ ($\Delta\Delta G\ddagger$) which we define as $\Delta\Delta G\ddagger = \Delta G\ddagger(MUT) - \Delta G\ddagger(WT)$. Translocation efficiency, ε, was also obtained from each translocation record by the relation, $\varepsilon = A_{obs}/A_{exp}$, where A_{obs} is the observed amplitude of channels that reopened (or translocated), and A_{exp} is the expected amplitude if all of the channels reopened (or translocated).

Chapter 3

Monitoring hydrophobic/steric ratchet transitions at the ϕ clamp

3.1 Introduction

How proteins are either translocated across or inserted into lipid bilayers is a fundamental and ubiquitous process in the cell. Transmembrane protein translocation plays key roles in pathology and normal cellular physiology. Structural studies have shown that translocase machinery is composed of an oligomeric protein complex, containing a central channel that the substrate polypeptide translocates through. These translocase systems use external sources of free energy to do work on their substrate. Typically, a protein substrate must initiate and thread into the translocase's central pore, then be forcibly unfolded, and finally be translocated directionally through the pore. Current research efforts are focused on the question of how translocases rectify and convert external electrochemical energy gradients into biased, directional force for unfolding and translocating substrates (Brown et al., 2011; Feld et al., 2012).

Thermal energy is significant at the molecular scale of translocase machines, thus it is critical that translocases have a mechanism to mitigate non-productive diffusion. Without a method to prevent backsliding, retrograde diffusive forces could counteract productive translocation or cause the translocase to slip when the driving force momentarily subsides. Ratchets, which restrict movement in one direction, are a way to ensure directionality in a mechanical system. Likewise, ratchet features in protein translocases could favor transport in one direction over another.

Translocases make use of different types of ratchets depending on their power source. Machines that use the proton motive force (PMF), like Anthrax toxin Protective Antigen (PA), can drive translocation by means of a charge-state ratchet mechanism (Krantz et al., 2006; Brown et al., 2011). The differential protonation of acidic residues in the substrate can allow protonated residues to pass through the cation selective channel; however, when these residues are depotonated on the higher pH side of the membrane, the substrate is productively trapped and unable to retrotranslocate back into the channel. Thus the PA channel is a protein-proton symporter, using protons to move protein across a membrane (Krantz et al., 2006; Finkelstein, 2008; Brown et al., 2011). Since translocation can be powered by a membrane potential in the absence of a proton gradient, the charge-state ratchet does not explain all of PA's translocase activity.

In Chapter 2, I presented evidence that PA can also use a hydrophobic ratchet mechanism to drive translocation. I discussed how the ϕ clamp plays a role in engaging substrates by binding hydrophobic/aromatic residues. We demonstrated that the ϕ clamp binds tightly to hydrophobic/aromatic sequences, and that this binding ultimately results in faster transport of folded domains. In this chapter, I will discuss how the ϕ clamp might disengage substrates, which is a necessary step for productive transport. We propose that that the ϕ clamp may modulate its affinity for substrates by switching between high- and low-affinity binding modes. The tight binding mode is important for unfolding substrates and preventing non-productive diffusion, as I discussed in Chapter 2; however switching to the low affinity state would prevent the substrate from binding too tightly to the ϕ clamp and allow translocation of the polypeptide. Crystallographic evidence, analyzed by my colleague Geoffrey Feld, demonstrates that the ϕ-clamp loop can adopt multiple conformations in the soluble form of PA. Single-channel

electrophysiology with hydrophobic/aromatic peptides reveals multiple, stable conformations of the channel-peptide complex. As the ϕ clamp is the site of current block and peptide binding, we propose the stable conformations we see are different states of the ϕ clamp, and we show that mutating the ϕ clamp shifts the population of the intermediates. Finally, we provide preliminary data that restricting the dynamics of loops in the channel results in altered transport of peptides and proteins. We believe our data support the hypothesis that the PA ϕ clamp operates as a tunable, hydrophobic/steric ratchet system to drive protein unfolding and translocation.

3.2 Results

Crystallographic analysis of translocase active site loops. My colleague Geoffrey Feld performed an analysis of known PA prechannel crystal structures, which revealed that the two major loops involved in PA driven translocation can adopt multiple conformations (Lacy et al., 2004; Kintzer et al., 2009; Feld et al., 2010). The ϕ-clamp loop, which contains the catalytic Phe-427 residue; and $Loop_{397}$, which is located above the ϕ-clamp loop and has been hypothesized to interact with the ϕ-clamp loop via a salt bridge between Lys-397 and Asp-426, were observed in two distinct conformations (Krantz et al., 2005; Melnyk and Collier, 2006) (Figure 3.1). In the ligand-free structure of PA_8 (Protein Data Bank 3HVD), both the ϕ-clamp loop and $Loop_{397}$ are tilted upward, relative to the $PA_8(LF_N)_4$ structure (3KWV) and the PA_7 structure (1TZO). It appears as if the conformations of the two loops are coordinated, since a $Loop_{397}$ in the *down* conformation would sterically clash with a ϕ-clamp loop in the *up* conformation. Though these structures are not of PA channels, inter-loop salt bridge evidence supports the idea of coordinated loop movement in the channel state (Melnyk and Collier, 2006). We hypothesize that the different loop conformations may represent alternate binding states of the ϕ clamp, which could enable the ϕ clamp to tune affinity in a driving-force dependent manner, provided one binding site had a reduced affinity for substrate. Transitions between the two ϕ-clamp states could promote substrate unfolding without limiting translocation.

Using small peptides to probe ϕ clamp interactions. We designed a series of small peptides to functionally probe the interaction of the ϕ clamp and $Loop_{397}$ sites with a translocating sequence. Each probe had a conserved pattern of residues; 5 N-terminal lysines ensure directional entry into the channel, and the remaining 5 residues contained the guest sequence in a XXSXX pattern (Figure 3.2A). We identify the peptides by the 3-letter code for the guest residue, e.g. Thr peptide has the sequence KKKKKTTSTT. We prepared representative probes for each category of amino acid, except charged residues. We kept the total charge constant for all peptides because we wished to avoid intermingling the study of hydrophobic ratcheting with any possible effects of charge-state ratcheting. We established in Chapter 2 that these probes specifically bind the ϕ clamp in a sequence and force dependent manner.

In an attempt to functionally confirm the multiple states of the ϕ-clamp loop we observed in crystal structures, we investigated the dynamics of the ϕ clamp/peptide interaction using these probes and single-channel electrophysiology. In these experiments a single PA channel is inserted in a lipid bilayer and peptide is added to one side of the membrane at ~20 nM. Channel openings and closings, which correspond to binding and unbinding events, are recorded. We were able to identify the expected open and peptide-bound states of the channel as well as two additional, partially open states, when we conducted experiments at +20 mV. We observe the two novel intermediate subconductance states of the channel, which we are calling I_1 and I_2,

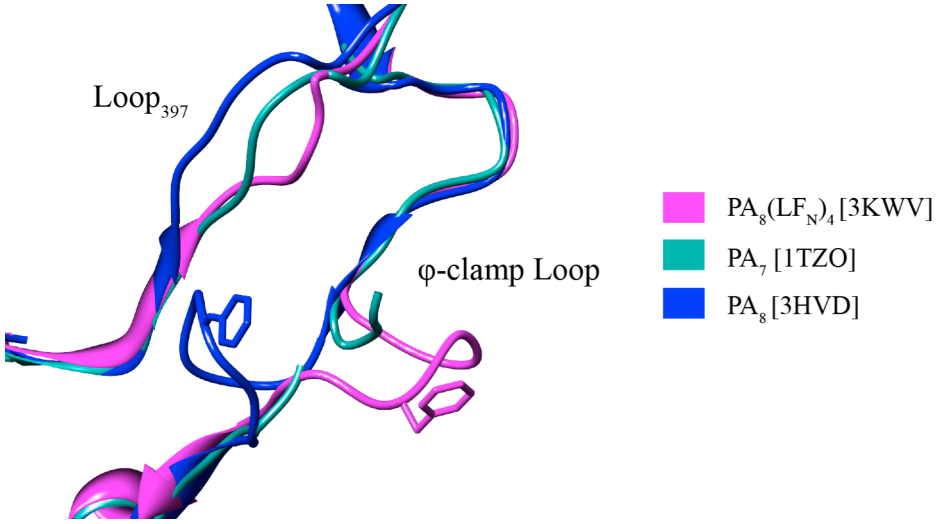

Figure 3.1. PA pore loops are flexible. My colleague Geoffrey Feld preformed an analysis of known X-ray crystal structures of the soluble PA prechannel and found multiple conformations of two important pore loops (Lacy et al., 2004; Kintzer et al., 2009; Feld et al., 2010). In the ligand-free structure of PA_8 (blue), both the ϕ-clamp loop and $Loop_{397}$ are tilted upward, relative to the $PA_8(LF_N)_4$ structure (magenta) and the PA_7 structure (teal). These loops may be linked by a salt bridge that has been reported to form upon channel conversion (Melnyk and Collier, 2006). This salt bridge may provide a means to coordinate the conformations of the two loops, since a $Loop_{397}$ in the down conformation would sterically clash with a ϕ-clamp loop in the up conformation.

primarily with large hydrophobic peptides, though they are occasionally observed with small hydrophilic sequences (Figure 3.2B).

Population of intermediates is driving-force dependent. Our initial experiments were conducted at +20 mV, and at this $\Delta\Psi$, the intermediates are only significantly populated by aromatic peptides (Figure 3.2B). We extended our analysis to +70 mV and observed intermediates with all peptides, though population of the intermediates was still enriched with aromatic peptide sequences (Figure 3.3). We believe that the relationship between increased $\Delta\Psi$ and increased intermediate state population indicates that the intermediates are a part of the translocation pathway, as we established in Chapter 2 that at +70 mV, the peptides are being translocated through the channel.

Intermediates are largely a product of the channel. We next asked whether the intermediates were a function of the peptides or of the channel itself. We analyzed single-channel data for all 6 peptides with WT PA and measured conductance values for the intermediate states at +70 mV. We found that I_1 and I_2 were clearly distinct from one another and from open and bound states, regardless of the peptide sequence (Figure 3.4). Within each intermediate state we did observe a trend where the conductance we measured was inversely correlated with the size of the peptide; small peptides had the largest conductance, large peptides had the smallest conductance (Figure 3.4). These results indicate that the size of the peptide plays a role in the intermediate conductance, but that this is not sufficient to explain the intermediates. We asked whether the intermediates were due to peptide conformation by testing a Trp peptide made with alternating D, L amino acids (D,L-Trp). By virtue of this, D,L-Trp should not be able to adopt conformations similar to the all-L peptides, like α helix. We found that D,L-Trp displayed intermediates I_1 and I_2 with WT PA, identical to L-Trp (Figure 3.4).

In Chapter 2, we established that peptide binding to the ϕ clamp creates current block. The intermediates we observe are a subset of current block, thus we wanted to determine the extent to which the ϕ clamp is responsible for generating the intermediates. We mutated F427, the catalytic ϕ-clamp residue, and asked whether the intermediates were still present. We found that both F427A and F427Y clamps shifted the equilibrium to favor the intermediate states at +70 mV, for all peptides (Figure 3.5A). Furthermore, we observed the intermediates for all peptides at low $\Delta\Psi$ (Figure 3.5B). We rarely observed the fully blocked state with either mutant ϕ clamp, regardless of $\Delta\Psi$, which provides evidence that the fully blocked state is the fully bound WT ϕ clamp/peptide complex, and that the stability of this complex is partially dependent on F427.

Finally, we compared the conductance values for all intermediates across all ϕ-clamp mutants, at +70 mV. F427Y and F427A channels have a larger unitary conductance than WT PA, but conductance is a product of more than pore size, since F427Y should have a smaller pore than the WT clamp. Based on these results, conductance likely reflects a combination of pore size and the hydrophobicity of the K^+ ion constriction point, which is the ϕ clamp. We averaged the conductance values we obtained for all the peptides with each PA mutant and found that I_1 did not scale with channel conductance, while I_2 did (Figure 3.5C). As we showed in Figure 3.4, the intermediates are a product of the channel and the peptide; thus the conductance we measure is a product of the full (open) channel conductance being blocked by a peptide. I_1, which does not scale with ϕ-clamp mutant conductance, may represent an alternate bound peptide/ϕ-clamp loop conformation. I_2, which does scale with the open channel conformation, may reflect a state in which the peptide is not actually bound at the ϕ clamp, which would allow for the ϕ-clamp mutant induced current increase.

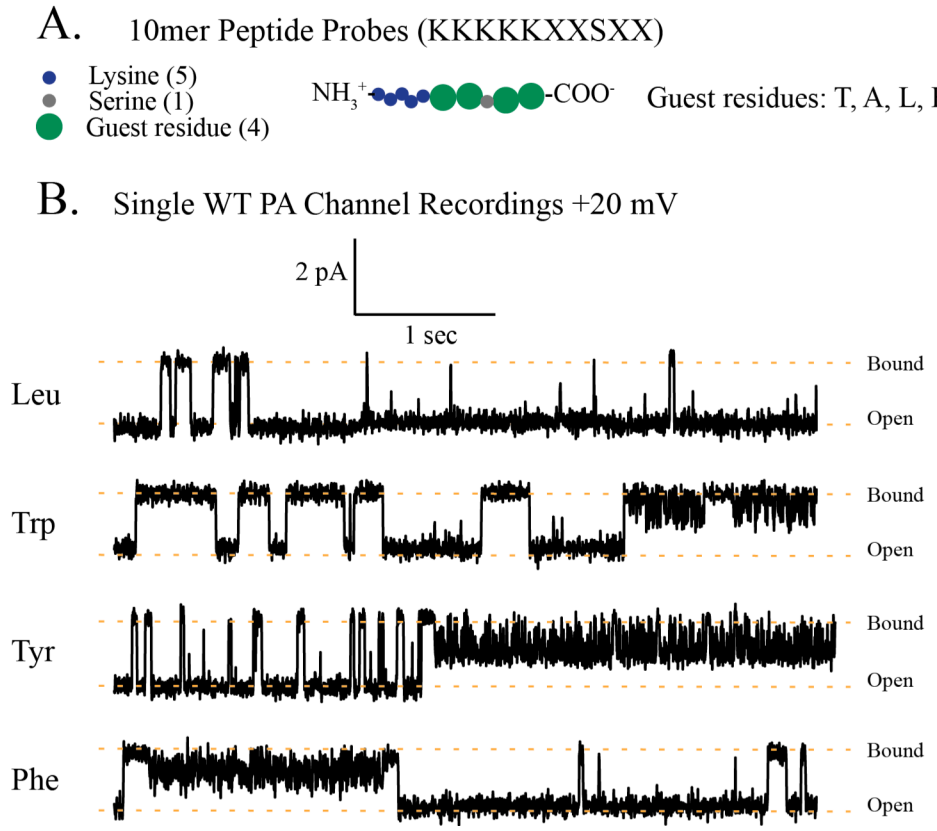

Figure 3.2. Peptide probes report on the ϕ clamp. (A) Diagram depicting our host-guest synthetic peptide probes. Each probe has 10 residues; the 5 N-terminal Lys residues provide directionality, the 5 C-terminal residues contain the guest residue of interest in a conserved XXSXX pattern. The peptides are identified by the 3-letter code for the guest residue, e.g. Thr peptide has the sequence KKKKKTTSTT. **(B)** Single channel recordings show WT PA interacting with representative peptides at +20 mV. We observe open and closed states of the channel, which correspond to peptide free and peptide bound, respectively. We also see intermediate current states with hydrophobic/aromatic sequences, that we do not observe with purely hydrophobic sequences, like Leu.

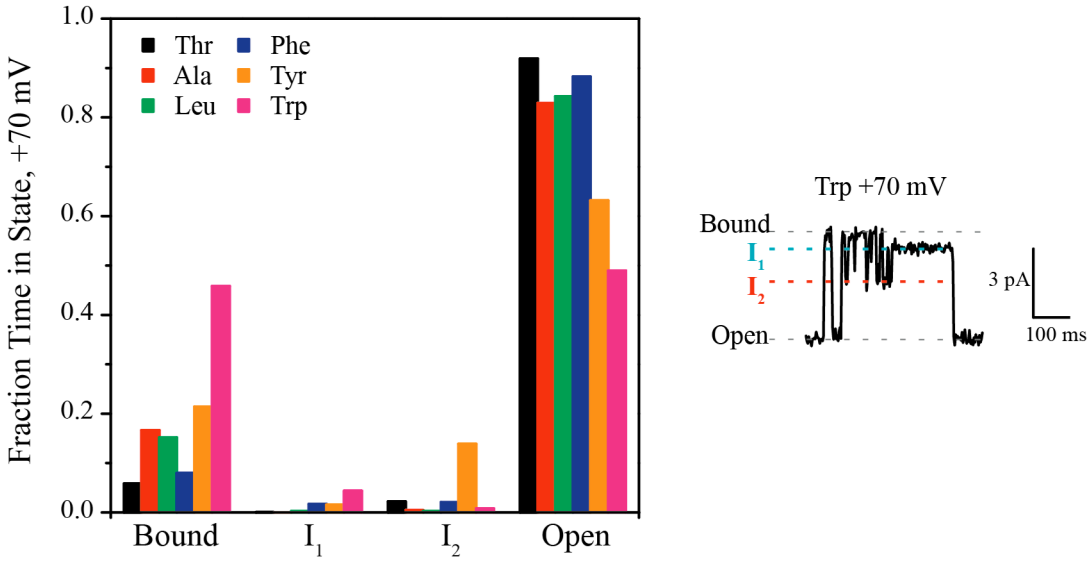

Figure 3.3. All peptides occupy intermediate states at high ΔΨ. We measured the fraction of time each peptide spends in each of the 4 states of the channel (open, bound, I_1, I_2). The diagram on the right depicts the 4 states, as measured with Trp peptide. At +70 mV, which is well within the translocation regime, we observe peptide-channel complexes in the intermediate states. The most hydrophobic/aromatic sequences occupy the intermediates most frequently, as indicated by the column graph. These data were collected with single WT PA channels.

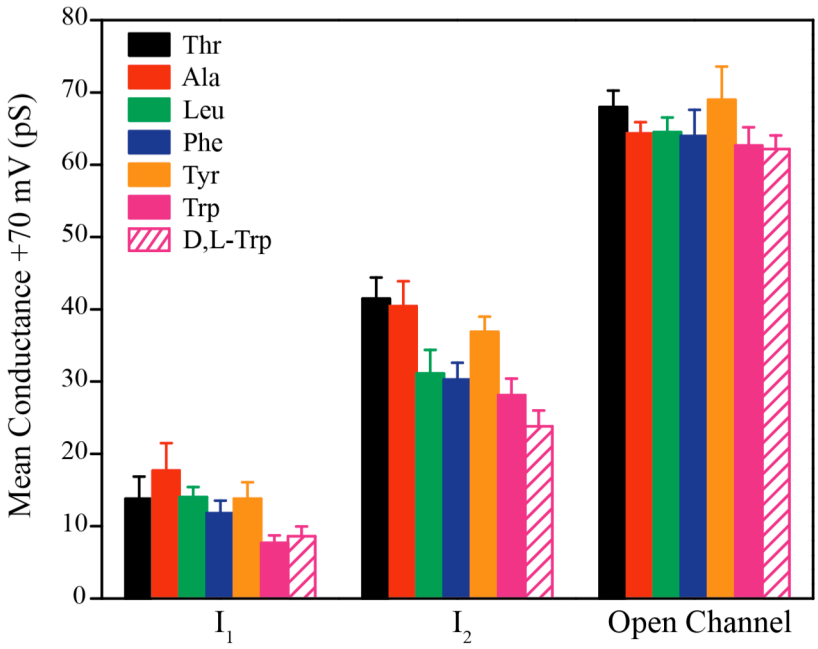

Figure 3.4. Intermediate states are not a product of peptide chemistry or α-helical conformation. We measured the conductance at each of the 4 states for single WT PA channels in complex with peptides. Conductance is a measure of ion flow, defined as current/voltage. Both intermediate states show a trend where the larger substrates result in less conductance, which indicates that the intermediates are peptide-channel complexes. We also see that I_1 is distinct from I_2, regardless of peptide. The open channel conductance is included as a control, as there is no statistically significant variation. We assayed an additional peptide, D,L-Trp, to confirm that peptide structure was not a contributing factor. D,L-Trp is conformationally restricted due to an every-other-residue chirality change, thus it should not be able to adopt conformations, like α-helix, that are available to all-L peptides. We observed no conductance differences in the intermediate states for D,L-Trp and L-Trp, thus we conclude that the intermediates are not likely to be related to a specific peptide conformation, and that the intermediates may be a product of conformational changes at the peptide binding site in the channel.

Our single-channel experiments have established that when peptides bind to the ϕ-clamp site they block the flow of current. The intermediate conductance states we discovered are a subset of the fully blocked state. Finally, the population of the intermediate states is dependent on F427 and driving force. Our results do not support the hypothesis that the intermediates are a product of unique peptide conformations. Instead, we hypothesize that the intermediates we observe correspond to different conformations of the ϕ clamp, which is consistent with our results.

Observation of committed kinetic steps in PA's translocation mechanism. We wanted to fully investigate the translocation pathway we observed at high ΔΨ with WT PA and Trp peptide. We chose to focus on Trp peptide because we had previously found that it interacted most tightly with the ϕ clamp, thus we predicted it would be easiest to work with, as most transitions out of the bound state were slow. We measured rates for the 12 possible transitions between open, bound, and the two intermediate states of the channel by plotting peptide dwell times at each state as cumulative distribution functions and then fitting the data to single or double exponentials.

We discovered a distinct pathway, where binding events were followed by transitions between the blocked state, I_2, and I_1; and then from I_1 to an open channel (Figure 3.6A). For Trp, we conclude that I_1 is on the translocation pathway; as in 75% of cases, peptide translocation is preceded by a dwell at I_1 of >10 ms, which we are a calling a stable dwell. The 25% of cases that transition directly from bound to open are likely an artifact of short dwell times in I_1, as evidenced by the multi-exponential fit of the bound-open CDFs. Transitions out of the stable dwell at I_1 to any state other than open are rare, so we hypothesize that establishing the stable dwell at I_1 represents a committed step in the translocation pathway. Our results indicate that I_2 is off the translocation pathway for Trp peptide, as peptides in I_2 are never directly transitioned to the open (translocated) state. We found that simple peptides, like Leu, have a less complicated translocation pathway, with most transitions observed between the bound and open states, with little time spent in the intermediates (Figure 3.6B).

Two possibilities could explain our data; (i) most peptides do not dwell in intermediates, (ii) we can only observe the intermediate dwells with bulky peptides. Because we occasionally observe short dwells for even our smallest peptides, we can discount the second possibility. We hypothesize that the intermediates are less stable than the full-block state in the context of most peptides we tested and WT PA, but the hydrophobic/aromatic peptide-ϕ-clamp complex has increased stability at the intermediate states. When we mutate the ϕ clamp, we hypothesize that the fully bound state is destabilized, which leads to increased population of the intermediates. Our results are consistent with the hypothesis that the intermediates represent alternate conformations of the ϕ-clamp loop, where I_1 corresponds to a substrate bound state and I_2 corresponds to an unbound state. It is possible that the committed steps we observe in the translocation of large peptides like Trp represent ratchet transitions, where the ϕ-clamp loop changes conformation, causing a release of bound peptide. The peptide is then free to move through the channel in the direction of productive translocation, but is prevented from moving backward by a steric clash with the ϕ clamp. We favor a model in which the driving force regulates the conformational change at the ϕ clamp, perhaps through the $Loop_{397}$/ϕ-clamp loop salt bridge.

Loop dynamics alter peptide and protein translocation. Mutations at the ϕ clamp are useful for studying peptide transport, however, these mutant proteins are inefficient or incapable of translocating folded proteins (Krantz et al., 2005). We wanted to test our hypothesis that ϕ-

clamp loop dynamics are important for translocation of peptides and proteins but we could not manipulate the ϕ-clamp loop itself without altering channel formation. Instead, we made two different pairs of cysteine mutations in the $Loop_{397}$ (Figure 3.7A). In the first construct, PA_{LL}, we mutated L378 and L401 to cysteine, so when a disulfide bond forms between the two residues, the $Loop_{397}$ should be locked in the up position. In the second construct, PA_{LA}, we mutated L378 and A396 to cysteine, so when a disulfide bond forms between the two residues, the $Loop_{397}$ should be locked in the down position. We hoped that by restricting the conformation of the $Loop_{397}$ we would also restrict the available conformations for the ϕ-clamp loop. The loops have been previously hypothesized to function in tandem (Melnyk and Collier, 2006), and our crystallographic evidence suggests the loop conformations may be mutually exclusive.

We conducted a single channel kinetic analysis of the two PA disulfide mutants with Trp peptide under oxidizing and reducing conditions at +70 mV. In both cases, we observed the same intermediate states of the channel (Figure 3.7B). We normalized the rate constants for all the transitions we measured in the oxidized PA constructs to the rate constants we measured under reducing conditions (Figure 3.7C). The rates for many transitions were only slightly affected, however we observed an almost 3-fold rate increase for transitions between bound and unbound states via I_1 in PA_{LL}. PA_{LA} was about 2-fold slower in the oxidized state for the same transition. Though we do not have direct evidence to demonstrate disulfide bond formation, the oxidized and reduced samples have different kinetic properties, which leads us to believe a crosslink has formed. Most of the effects we measured were less than 2-fold but we still consider our results meaningful as we have shown that restricting dynamics of the $Loop_{397}$ has an impact on the translocation of peptides by the ϕ clamp.

As we showed in Chapter 2, peptide probes translocate differently than folded proteins. We asked whether the PA_{LA} mutation had any effect on the translocation of the model substrate LF_N-Td-DTA, under symmetric pH 5.60 conditions and a $\Delta\Psi$ driving force. In Chapter 2, we showed that under these conditions, translocation of the DTA domain is rate limiting. Our preliminary results indicate that PA_{LA} translocates the model substrate about 3-fold slower than the reduced control (Figure 3.7D). These results are interesting given that PA_{LA} translocated Trp peptide less than 2-fold slower than the reduced control. The difference may be due to the identity of the guest sequence, or it could be the difference between a peptide and a folded domain. Our results are preliminary and we plan to continue this line of investigation by translocating our folded substrates with PA_{LL}, and by measuring the effects of both PA mutants on translocation of LF_N-Wd-DTA. Still, our preliminary results support the hypothesis that the ϕ-clamp loop can sample multiple conformations, and that loop dynamics affect substrate unfolding and translocation.

3.3 Discussion

Hydrophobic gaskets are a common motif in translocase channels; they provide important interaction sites for substrates and play roles in force transduction. Here we investigated the ratcheting activity of the ϕ clamp, the hydrophobic gasket from PA. We have previously established that the ϕ clamp binds tightly to hydrophobic/aromatic sequences, and that this interaction slows transport of peptides yet increases transport rates of folded proteins. In this chapter, I have presented evidence to support the hypothesis that that the ϕ clamp may modulate its affinity for substrates by switching between high and low affinity binding states; I have also demonstrated committed steps in the translocation pathway for a hydrophobic/aromatic peptide.

A.

Fold Change in Time at State (F427X/WT)

	Thr		Ala		Leu	
	F427A	F427Y	F427A	F427Y	F427A	F427Y
Bound	0.30	1.03	0.39	0.33	0.02	0.22
I_1	6.86	1.66	743.30	4.75	7.86	3.37
I_2	0.31	0.23	0.35	0.32	2.37	1.48
Open	1.06	1.02	1.05	1.14	1.15	1.13

	Phe		Tyr		Trp	
	F427A	F427Y	F427A	F427Y	F427A	F427Y
Bound	0.14	0.65	0.09	0.18	0.00	0.09
I_1	2.48	1.26	9.83	2.90	2.33	1.61
I_2	0.69	0.93	1.82	1.31	3.31	3.63
Open	1.06	1.03	0.91	1.16	1.77	1.75

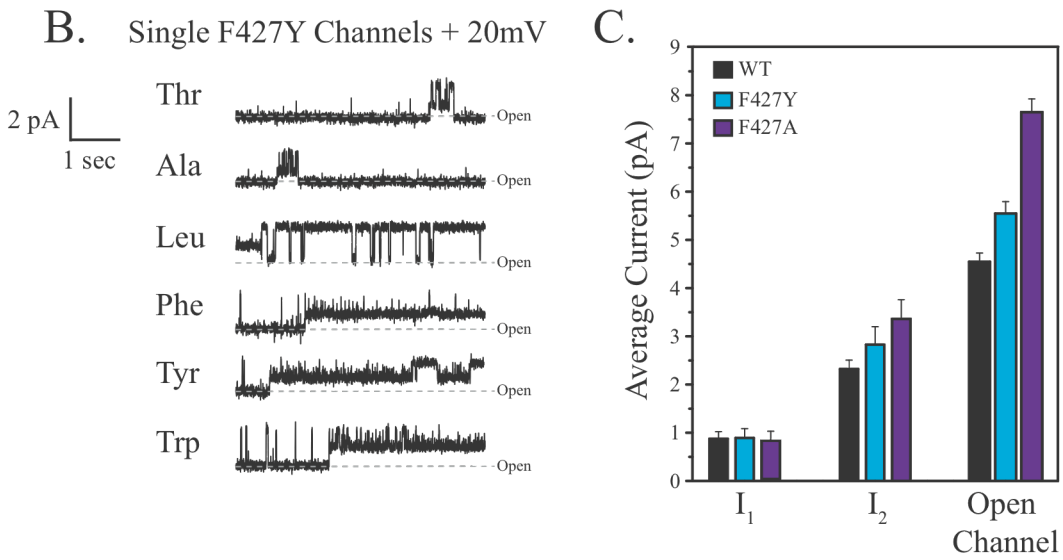

Figure 3.5. ϕ-clamp mutations increase population of the intermediate states. We mutated F427 to test whether the ϕ clamp was responsible for creating the intermediates. **(A)** We found that both F427A and F427Y mutations caused an increase in the fraction of time that peptides spent in the intermediate states, and a decrease in the time spent in the fully bound state, relative to WT, at +70 mV. **(B)** We observed intermediates at +20 mV for all peptides with PA F427Y. **(C)** We pooled the data for the amount of current measured at +70 mV for each state then averaged it to create a cumulative value that encompassed all peptide data for each PA construct. We found that F427 mutants were more conducting than WT channels in the open and I_2 states, but not in I_1. The intermediate conductance states are a product of the open channel conductance being partially occluded by the peptide substrate, and the open channel conductance reflects both the pore size and the hydrophobicity of the ϕ-clamp residue. I_1, which *does not* scale with the F427 mutations, may reflect a peptide-ϕ-clamp complex. I_2, which *does* scale with the open channel conductance, may reflect a state in which the peptide is not bound at the ϕ clamp.

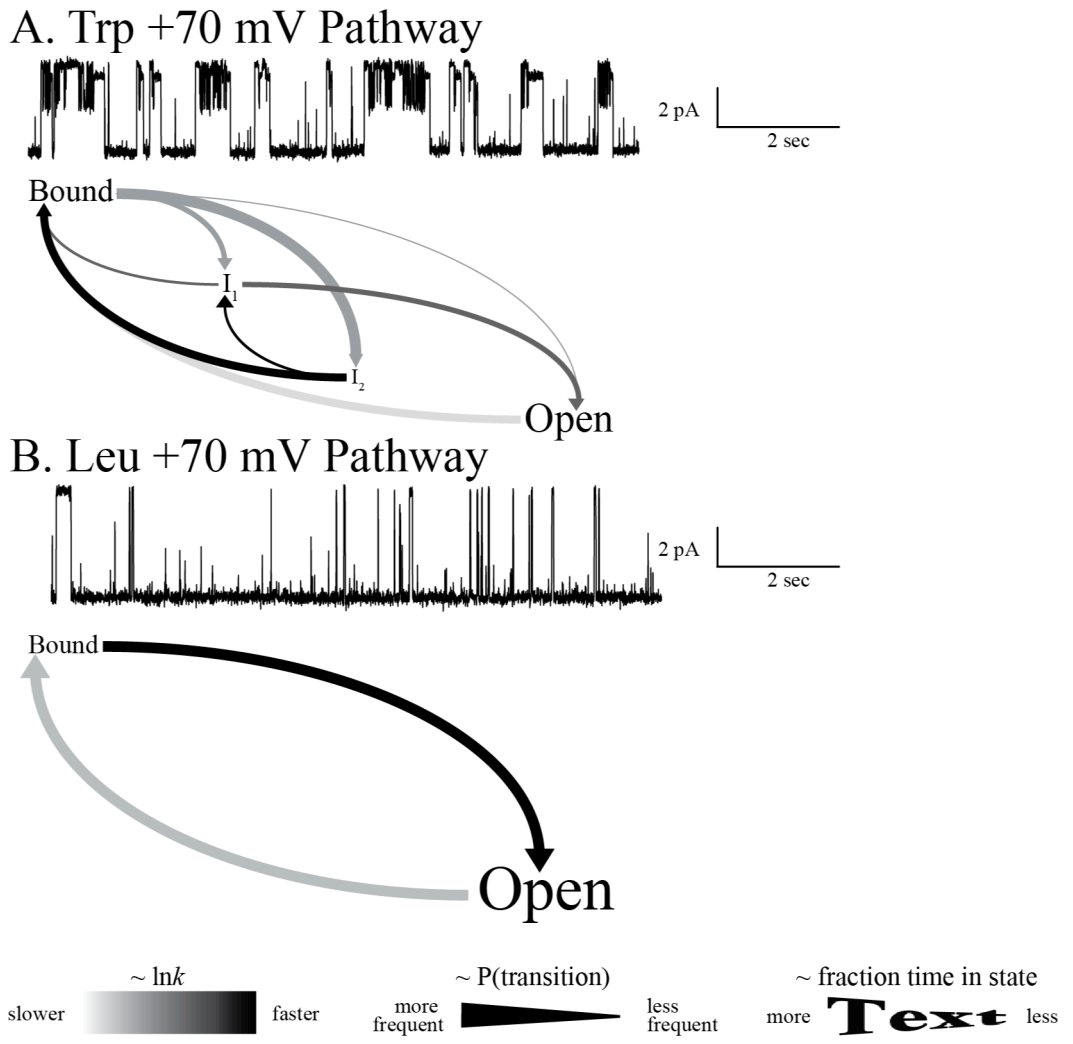

Figure 3.6. Hydrophobic/aromatic peptide translocation pathways have committed steps. **(A)** Trp peptide translocation pathway as measured with WT PA at +70 mV. This peptide has a complicated pathway, with many transitions between intermediate states and the bound state. Most Trp translocation events proceed from bound to I_1 to open, thus we consider that transition from I_1 to open a committed step in the translocation pathway. Once a stable dwell at I_1 is established, Trp peptides do not return to the bound state, though we occasionally observe rapid oscillations between bound and I_1. **(B)** Leu peptide has a very simple translocation pathway with WT PA at +70 mV, with less than 0.5% of transitions occurring to or from intermediate states. We do not observe the I_1 dwell for simple peptides like Leu, but we do for hydrophobic/aromatic peptides like Trp, Tyr, and Phe.

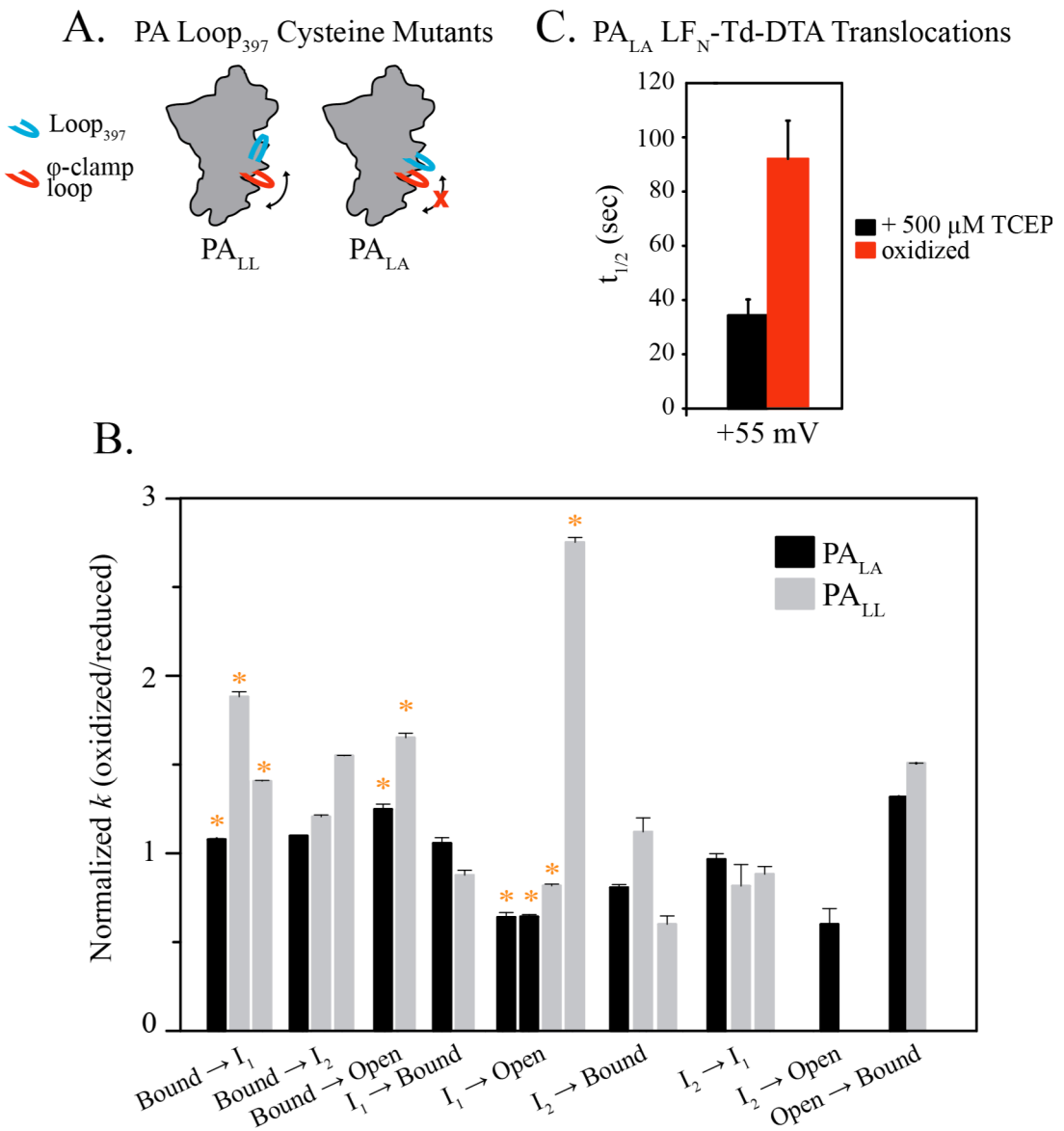

Figure 3.7. Restricting channel loop dynamics alters translocation kinetics. (A) We made two constructs with cysteine mutants placed in $Loop_{397}$ and the body of PA that should restrict the dynamics of $Loop_{397}$, and consequently the ϕ-clamp loop, upon disulfide bond formation. PA_{LL} has L378C and L401C mutations, which should lock $Loop_{397}$ in the up position. PA_{LA} has L378C and A396C mutations, which should lock $Loop_{397}$ in the down position, and reduce the likelihood that the ϕ-clamp loop would occupy the up position. **(B)** We translocated Trp peptide at +70 mV with the two PA mutants under oxidizing and reducing conditions and normalized the rate constants for each transition to determine fold change. Transitions on the translocation pathway for Trp peptide, indicated by orange stars, showed the greatest effects. Additionally, many PA_{LL} transitions were best fit with double exponentials, as opposed to the standard single exponential function. **(C)** We translocated LF_N-Td-DTA with PA_{LA}, at +55 mV and symmetric pH 5.60. We found that oxidized PA_{LA} translocated about 3-fold slower than the reduced control.

We hypothesize that the tight binding state of the ϕ clamp would be important for unfolding substrates and preventing non-productive diffusion; however, switching to the low affinity state would prevent the substrate from binding too tightly to the ϕ clamp and would favor translocation of the polypeptide. We favor a model in which the affinity at the ϕ clamp is regulated by driving force; when the force is high the affinity is low, which allows productive translocation, when the force is low the affinity is high, which favors unfolding and prevents backsliding. In our model the ϕ clamp itself provides a steric restriction to prevent retro-translocation of bulky sequences. We propose that the committed steps we observe during Trp peptide translocation, for example, represent ratchet transitions, and that the ϕ clamp achieves this ratcheting effect by adopting different conformations that have different substrate affinities. We propose a model in which the substrate/ϕ-clamp interaction reduces the barrier for substrate unfolding while simultaneously preventing counterproductive retrograde movement of the polypeptide chain. A hydrophobic ratcheting mechanism like what we propose here is compatible with any translocase system that has a hydrophobic/aromatic pore ring.

Crystallographic analysis of translocase active site loops. My colleague Geoffrey Feld preformed an analysis of previously collected PA pre-channel crystal structures, which revealed that the ϕ-clamp loop and $Loop_{397}$ can adopt multiple conformations (Figure 3.1). Each loop has an up and a down conformation, relative to the channel axis, and both loops have been implicated in the translocation mechanism (Krantz et al., 2005; Melnyk and Collier, 2006). $Loop_{397}$ in the down conformation could prevent the ϕ-clamp loop from adopting the up conformation, as the loops would sterically clash. A salt-bridge between Lys-397 and Asp-426, which forms upon conversion to the channel state, been reported to link $Loop_{397}$ to the ϕ-clamp loop, and be important for efficient translocation (Melnyk and Collier, 2006). The linkage between these two loops provides a mechanism for propagation of conformational changes within the channel.

We hypothesize that the flexibility of the pore loops could be a mechanism to modulate affinity for substrate. If one loop conformation had a higher substrate affinity than the alternate conformation, the channel could regulate affinity by alternating between the two states. The salt-bridge that has been reported to link the two loops could act as a pH sensor, regulating the linkage and thus modulating the loop conformation in a proton dependent manner. As the PMF is the physiological driving force for PA translocation, this salt bridge might be the mechanism by which the driving force regulates affinity at the ϕ clamp.

Why would the channel want to modulate its affinity for substrate? We know that the ϕ clamp forms an iris, or hydrophobic gasket, in the center of the channel, and that it provides a hydrophobic interaction surface and binds tightly to hydrophobic/aromatic sequences in substrates (Krantz et al., 2005). If the interaction, which we hypothesize is important for substrate unfolding, is too strong, the available driving force may not be able to break it, which would stall translocation. If the ϕ clamp could temporarily alter conformation to disengage the aromatic/hydrophobic sequence and allow it to pass though the pore, the substrate could be productively translocated. We favor a model where ϕ clamp affinity for substrate is regulated by driving force; when force is applied affinity for the substrate decreases, when the force subsides, affinity for the substrate increases. Once the ϕ clamp has altered conformation to release substrate, it could return to the original conformation, which would restrict the retrograde movement of the substrate due to a steric clash between the clamp and the just translocated hydrophobic/aromatic residue. This would be an especially useful mechanism to mitigate diffusive motion if the driving force was temporarily reduced.

Single channel electrophysiology reveals multiple states of the ϕ clamp. We used a series of 10 residue peptides that specifically bind the ϕ clamp to probe the state of the clamp. We recorded the conductance of single PA channels in the presence of 20 nM peptide at +20 mV, which revealed 4 distinct conductance states (Figure 3.2B). We observed conductance states corresponding to an open channel, a fully bound state, as well as two stable intermediate states that we identify as I_1 and I_2. At +20 mV only the hydrophobic/aromatic peptides dwell in the intermediate states, but at +70 mV all six peptides dwell at the intermediates (Figure 3.3). We observed the greatest fraction of intermediate state dwells with hydrophobic/aromatic peptides at all voltages we tested.

We wanted to distinguish between two hypotheses explaining the presence of intermediates, (i) they are a product of the peptide-ϕ-clamp complex adopting a specific conformation; (ii) they are a fundamental property of the channel. To test hypothesis (i) we compared the conductance states of the six standard peptides to a Trp peptide made with alternating D, L amino acids (D,L-Trp). D,L-Trp should be unable to adopt conformations available to all-L peptides, such as the α-helix. We observed identical conductance states for D,L-Trp and the other 6 peptides, which led us to discount our first hypothesis (Figure 3.4).

We then evaluated the second hypothesis, that the intermediates are a product of some structure in the channel. From previous experiments, we knew the hydrophobic/aromatic peptides were binding specifically to the ϕ clamp, and we found that these peptides also spent more time in the intermediate states. Based on that evidence, and our crystallographic analysis, we hypothesized that the intermediate conductance states represented alternate conformations of the ϕ clamp.

We made mutations at F427, the catalytic ϕ-clamp residue, and asked whether the intermediates were still present. We found that both F427A and F427Y clamps shifted the equilibrium to favor the intermediate states, for all peptides, and we rarely observed the fully bound state (Figure 3.5A, Figure 3.5B). These data indicate that in the WT ϕ clamp, F427 interacts with the peptides and the fully blocked state corresponds to this interaction. When we mutated F427, we disrupted the complex, and the system responded by increasing occupancy of the intermediate states. We interpret this to mean that the intermediates are less stable states of the ϕ-clamp loop/peptide complex, in the context of WT PA. We plan to calculate equilibrium constants for each of the intermediate states based on a partition function and the state-population data that we presented here.

We compared the conductance values for all intermediates across all ϕ-clamp mutants, at +70 mV, to test the dependence of conductance on F427. F427Y and F427A channels have a larger unitary conductance than WT PA, which means that conductance through the pore is a product pore size and the hydrophobicity of the K^+ ion constriction site (ϕ clamp). We averaged the values we obtained for the intermediates with all the peptides and found that I_1 did not scale with channel conductance, while I_2 did (Figure 3.5C). We hypothesize that I_2, which scales with the open channel, may correspond to peptide near but not bound to the ϕ clamp. We speculate that I_1 may represent an alternate conformation of the peptide-ϕ-clamp complex, which could explain why we don't see a current increase in the F427 mutants.

All the results I have presented support the hypothesis that the intermediates are a product of the ϕ-clamp loop adopting different conformations in the presence of peptides. Deleting the ϕ-clamp loop renders the channel nonfunctional, so the best way to directly test this hypothesis would be to monitor the position of the ϕ-clamp loop, and correlate positional changes with

binding of substrate or protons. We plan to undertake these experiments at some point in the future, but to date we have been unable to design an electrophysiology experiment that would disprove our hypothesis.

The peptide translocation pathway proceeds via an intermediate ϕ-clamp state and involves committed steps. In Chapter 2 we established that at +70 mV, the test peptides are translocating though the channel. We mapped the translocation pathway of Trp at +70 mV with WT PA. We found that translocation nearly always occurs via I_1, with very few transitions directly between bound and open states (Figure 3.6A). It is likely that the rare bound to open transitions we observe did proceed via I_1 but the dwell at I_1 was too short for our instruments or software to measure. As I discussed in chapter 2, the CDF fits for direct Trp translocation are not perfect single exponentials, which supports the idea that the translocation pathway is not a single step from peptide bound to open. In comparison, the Leu translocation pathway occurs directly between the bound and open states, with little time spent in the intermediates (Figure 3.6B).

In the case of Trp, translocation usually proceeds with a dwell at the blocked state, followed by a dwell at I_1, and finally a transition to the open channel. Because we rarely observe transitions from a stable dwell at I_1 to any state other than open, we propose that it could represent a committed step in the Trp translocation pathway. If, as we proposed, I_1 is an alternate state of the ϕ clamp/peptide complex, our results would indicate that we are directly observing a transition between a translocation incompetent complex (bound) and a competent complex (I_1), and that translocation proceeds via a conformational change in the ϕ clamp. Though we have little hard evidence to support this hypothesis, we do primarily observe the intermediates with hydrophobic/aromatic peptides. This is what we would expect if the transitions were indeed the ratchet 'release' events for bulky sequences.

Restricting $Loop_{397}$ dynamics alters peptide and protein translocation. We also wanted to test the functional consequences of the different proposed ϕ-clamp conformations. We had previously hypothesized that the dynamic nature of the loop was important for function, so ideally, we would restrict the conformation of the ϕ-clamp loop and then measure changes in translocation kinetics or single channel intermediates. However, we can not remove the ϕ-clamp loop itself without disrupting PA channel formation. Instead, we restricted the conformation of $Loop_{397}$. Functional and crystallographic evidence suggest that forcing Loop397 to adopt the down conformation may cause the ϕ-clamp loop to preferentially adopt the down conformation. We made two different pairs of cysteine mutations in the $Loop_{397}$ (Figure 3.7A). In the first construct, PA_{LL}, we mutated L378 and L401 to cysteine, so when a disulfide bond forms between the two residues, $Loop_{397}$ should be locked in the up position. In the second construct, PA_{LA}, we mutated L378 and A396 to cysteine, so when a disulfide bond forms between the two residues, $Loop_{397}$ should be locked in the down position. The ϕ-clamp loop should be preferentially occupy the down position in PA_{LA}.

We conducted a single channel kinetic analysis of the two PA disulfide mutants with Trp peptide under oxidizing and reducing conditions at +70 mV. In both cases, we observed the same intermediate states of the channel (Figure 3.7A). This result was unexpected, but without crystal structures of the disulfide mutants to confirm the position of the ϕ-clamp loop, we can't exclude the possibility that the ϕ-clamp loop can still access both conformations. Because we see differences between oxidized PAs and the reduced controls, we are fairly sure that the oxidized constructs are indeed oxidized.

We normalized the rate constants we measured in the oxidized PA constructs to the rate constants we measured under reducing conditions (Figure 3.7B). The rates for many transitions were only slightly affected, however we observed an almost 3-fold rate increase for transitions between bound and unbound states via I_1 in PA_{LL}, and a 2-fold decrease for PA_{LA}. Though most of the effects we measured were less than 2-fold, we believe the effects are meaningful, because we have demonstrated that restricting the conformation of the $Loop_{397}$ has an impact on the translocation of peptides by the ϕ clamp. Incomplete reduction of the disulfides could also skew the fold-increase.

We tested how the PA_{LL} and PA_{LA} mutations affected the translocation of the model substrate LF_N-Td-DTA, under symmetric pH 5.60 conditions and a $\Delta\Psi$ driving force. Under these conditions translocation of the DTA domain is rate limiting. Our preliminary results indicate that oxidized PA_{LA} translocates the model substrate about 3-fold slower than the reduced control (Figure 3.7C). Again, this effect is not large, but it is reproducible and statistically significant. We believe that optimization of experimental conditions could increase the fold-change we measure, and we will pursue this avenue in the future. It is also interesting to note that PA_{LA} translocated Trp peptide less than 2-fold slower, while it translocated LF_N-Td-DTA 3-fold slower. We intend to investigate whether this effect is due to the type of substrate or to the sequence of the substrate, likely by translocating Thr peptide and LF_N-Wd-DTA. We could also pursue mutations at different residues to ensure that we find the disulfide position that has the largest impact on loop mobility. Regardless, our translocation results provide more evidence that the ϕ-clamp loop can sample multiple conformations, and that loop dynamics affect substrate unfolding and translocation. We will also continue translocations with these substrates and PA_{LL}.

Hydrophobic/steric ratchet transitions at the ϕ clamp may drive translocation. We propose a model in which the ϕ-clamp loop and $Loop_{397}$ are coupled, and can adopt alternate conformations (Figure 3.8). Each conformation of the ϕ-clamp loop has a different affinity for substrate, which would allow the channel to regulate the ratchet behavior. We propose that cycles of high and low affinity binding would help unfold substrates, simultaneously prevent backsliding, all without slowing productive translocation. The tunable substrate affinity we propose would allow the channel to bind tightly to substrate when necessary for unfolding and subsequently release the substrate in order to bind the next bulky residue. We favor a model in which the ϕ-clamp affinity for substrate is regulated by driving force. When force is applied affinity for the substrate decreases, when the force subsides, affinity for the substrate increases; thus the driving force would be regulating the conformational changes that we propose occur at the ϕ clamp. Retrograde movement though the clamp is prohibited by a steric clash between released sequences and the ϕ clamp. Thus, we propose that the ϕ clamp acts as a hydrophobic/steric ratchet. An efficient translocation system could involve many different types of ratchet mechanisms. PA is no exception; in this one translocase we have identified hydrophobic and charge state ratchets, as well as other clamping sites that bind unfolded structures. Other protein conducting channels, including ATP-powered machines, could make use of similar ratcheting systems.

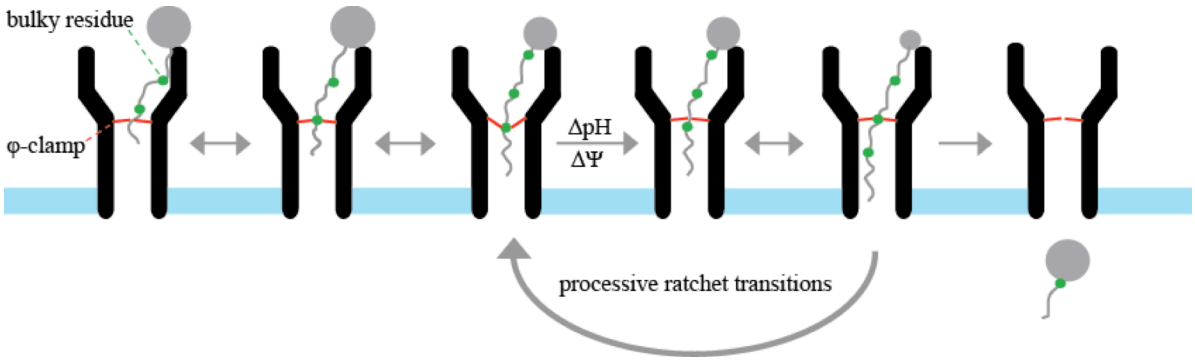

Figure 3.8. The ϕ clamp acts as a hydrophobic/steric ratchet to drive unfolding and translocation. In our model, the ϕ clamp binds bulky hydrophobic/aromatic residues in the substrate as they are exposed during the unfolding process. This favorable interaction lowers the barrier for substrate unfolding, but also temporarily slows translocation. The interaction is broken by a conformational change at the ϕ clamp, which reduces the affinity for the substrate, and allows the bulky residue to pass through the clamp. The ϕ clamp then resumes its high affinity position, which sterically occludes the bulky residue from retrotranslocating. We propose that driving force regulates the affinity; when force is high the affinity is low to allow translocation, when force subsides the affinity increases to prevent retrotranslocation. Processive ratchet transitions between high and low affinity states explains the seemingly contradictory results we have described; that the ϕ clamp binds bulky residues tightly, which slows peptide transport but increases transport of folded domains. Thus, we propose the ϕ clamp acts as a ratchet; catalyzing unfolding while simultaneously preventing backsliding, and that this activity is based upon conformational changes of the ϕ-clamp loop.

3.4 Materials and methods

Peptides. All 10mer oligopeptides were synthesized and purified to >95% (Elim Biopharmaceuticals, Hayward, CA). Peptides were dissolved in ultra pure H_2O and concentrations were determined using backbone and/or residue absorbance, when the sequence contained Tyr or Trp residues.

Proteins. WT and PA mutants were expressed, purified, and oligomerized as previously described (Thoren et al., 2009). PA_{LL} and PA_{LA} constructs were created using QuikChange mutagenesis. Reduced controls of these proteins were oligomerized and stored in DTT. His_6-LF_N-guest-peptide-DTA guest-host expression system was constructed from residues 1-263 of LF followed by the A chain of diphtheria toxin (DTA) sequence contained in a pET15b expression vector (Krantz et al., 2005). A Not I site located after the C terminus of LF_N and a Spe I site followed by a thrombin recognition site just before the N terminus of DTA were engineered into the pET15b construct. These unique restriction sites allowed insertion of a 25-residue guest peptide sequence. Not I/Spe I-flanked DNA cassettes encoding the desired guest peptide sequences were synthesized and cloned according to previously described gene synthesis methods (Feld et al., 2010; Brown et al., 2011). His_6-LF_N-guest-DTA proteins were purified from overexpressing bacteria using standard Ni^{2+}-nitrilotriacetic acid affinity chromatography and Blue Sepharose affinity (BS) chromatography. Proteins containing extremely hydrophobic guest sequences were isolated from inclusion bodies and further purified by BS chromatography.

Electrophysiology. Planar lipid bilayer currents were recorded using an Axopatch 200B amplifier (Molecular Devices Corp., Sunnyvale, CA) as described (Kintzer et al., 2009; Thoren et al., 2009). Membrane bilayers were painted onto a 100-μm aperture of a 1-ml delrin cup with 3% 1,2-diphytanoyl-sn-glycero-3-phosphocholine (Avanti Polar Lipids, Alabaster, AL) in neat *n*-decane. Cis (side to which the PA oligomer is added) and trans chambers were bathed in the indicated buffers as required. Experiments were conducted under a membrane potential, $\Delta\Psi \equiv \Psi_{cis} - \Psi_{trans}$ ($\Psi_{trans} \equiv 0$ V).

For ensemble peptide-binding electrophysiology, planar lipid bilayers were bathed in universal pH 5.60 bilayer buffer (UBB: 10 mM oxalic acid, 10 mM phosphoric acid, 10 mM MES, 1 mM EDTA). PA oligomers were added to the cis chamber under a $\Delta\Psi$ of +20 mV and allowed to form channels. When the total current in the experiment reached ~5000 pA excess PA was perfused away. The $\Delta\Psi$ was then adjusted in the range of -10 mV to +80 mV. Small aliquots of peptide were then added to the cis chamber and allowed to equilibrate. Binding of peptide to the channels resulted in blocking of the channel and a decrease in total current. The total concentration of peptide added and the fraction of channels still conducting were recorded until all channels were effectively blocked by peptide.

For single-channel peptide translocation, planar lipid bilayers were bathed in symmetric buffer (100 mM KCl, 1 mM EDTA, 10 mM succinic acid, pH 5.60). PA_7 oligomer was applied directly to membranes at 10^{-16} M. Single channel insertion was observed by a discrete increase in current under an applied voltage of +20 mV. Once a single channel had inserted into the membrane, peptide was added to the cis side of the membrane at 18-20 nM. Data were recorded at 400 or 600 Hz using a low pass filter of 200 Hz under varying applied $\Delta\Psi$. Reducing experiments were done in the presence of 500 μM TCEP, which is more active than DTT at pH 5.60.

For ensemble LF_N-guest-peptide-DTA translocation assays, translocation experiments were carried out using UBB at symmetric pH 5.60 as described (Kintzer et al., 2009; Thoren et al., 2009). Membranes were formed and channels were inserted as described for bulk peptide

binding experiments. His_6-LF_N-guest-peptide-DTA substrate was added to the cis-side of the membrane at 20 nM, and binding was monitored as a decrease in current. Excess substrate was removed by perfusion and the translocation process was initiated by increasing the $\Delta\Psi$. Reducing experiments were done in the presence of 500 μM TCEP.

Data Analysis. For single channel kinetic analysis, dwell times were extracted from datasets using the single channel tool in CLAMPFIT10.2 (Molecular Devices, Sunnyvale, CA). We excluded short duration (<7 ms) dwell times due to our data collection filtering settings. Dwell times were compiled into cumulative distribution functions (CDF) in MATLAB (MathWorks, Natick, MA). Each CDF was fit with a single exponential function [$y = y_0 - \exp(-\lambda * x)$], in ORIGIN (OriginLab, Northampton, MA) to determine rate constants (λ) for each observed transition. Protein translocation was quantified as the time for half the protein to translocate ($t_{1/2}$).

References

Alder, N.N., and Theg, S.M. (2003). Energetics of protein transport across biological membranes. a study of the thylakoid DeltapH-dependent/cpTat pathway. Cell *112*, 231–242.

Aubin-Tam, M.-E., Olivares, A.O., Sauer, R.T., Baker, T.A., and Lang, M.J. (2011). Single-molecule protein unfolding and translocation by an ATP-fueled proteolytic machine. Cell *145*, 257–267.

Banks, W.A. (2009). Characteristics of compounds that cross the blood-brain barrier. BMC Neurol *9 Suppl 1*, S3.

Barkow, S.R., Levchenko, I., Baker, T.A., and Sauer, R.T. (2009). Polypeptide translocation by the AAA+ ClpXP protease machine. Chemistry & Biology *16*, 605–612.

Basilio, D., Juris, S.J., Collier, R.J., and Finkelstein, A. (2009). Evidence for a proton-protein symport mechanism in the anthrax toxin channel. The Journal of General Physiology *133*, 307–314.

Blanke, S.R., Milne, J.C., Benson, E.L., and Collier, R.J. (1996). Fused polycationic peptide mediates delivery of diphtheria toxin A chain to the cytosol in the presence of anthrax protective antigen. Proc Natl Acad Sci USA *93*, 8437–8442.

Blaustein, R.O., Koehler, T.M., Collier, R.J., and Finkelstein, A. (1989). Anthrax toxin: channel-forming activity of protective antigen in planar phospholipid bilayers. Proc Natl Acad Sci USA *86*, 2209–2213.

Brown, M.J., Thoren, K.L., and Krantz, B.A. (2011). Charge requirements for proton gradient-driven translocation of anthrax toxin. J Biol Chem *286*, 23189–23199.

Chen, L.-M., Briones, G., Donis, R.O., and Galán, J.E. (2006). Optimization of the delivery of heterologous proteins by the Salmonella enterica serovar Typhimurium type III secretion system for vaccine development. Infect Immun *74*, 5826–5833.

Choy, J.S., Aung, L.L., and Karzai, A.W. (2007). Lon protease degrades transfer-messenger RNA-tagged proteins. J Bacteriol *189*, 6564–6571.

Collier, R. (2009). Membrane translocation by anthrax toxin. Mol Aspects Med.

De Los Rios, P., Ben-Zvi, A., Slutsky, O., Azem, A., and Goloubinoff, P. (2006). Hsp70 chaperones accelerate protein translocation and the unfolding of stable protein aggregates by entropic pulling. Proc Natl Acad Sci USA *103*, 6166–6171.

Driessen, A.J.M., and Nouwen, N. (2008). Protein translocation across the bacterial cytoplasmic membrane. Annu Rev Biochem *77*, 643–667.

Duesbery, N.S., Webb, C.P., Leppla, S.H., Gordon, V.M., Klimpel, K.R., Copeland, T.D., Ahn, N.G., Oskarsson, M.K., Fukasawa, K., Paull, K.D., et al. (1998). Proteolytic inactivation of

MAP-kinase-kinase by anthrax lethal factor. Science *280*, 734–737.

Eilers, M., and Schatz, G. (1986). Binding of a specific ligand inhibits import of a purified precursor protein into mitochondria. Nature *322*, 228–232.

Erlandson, K.J., Miller, S.B.M., Nam, Y., Osborne, A.R., Zimmer, J., and Rapoport, T.A. (2008). A role for the two-helix finger of the SecA ATPase in protein translocation. Nature *455*, 984–987.

Ezzell, J.W., and Abshire, T.G. (1992). Serum protease cleavage of Bacillus anthracis protective antigen. J. Gen. Microbiol. *138*, 543–549.

Falnes, P.O., Choe, S., Madshus, I.H., Wilson, B.A., and Olsnes, S. (1994). Inhibition of membrane translocation of diphtheria toxin A-fragment by internal disulfide bridges. J Biol Chem *269*, 8402–8407.

Feld, G.K., Brown, M.J., and Krantz, B.A. (2012). Ratcheting up protein translocation with anthrax toxin. Protein Sci.

Feld, G.K., Thoren, K.L., Kintzer, A.F., Sterling, H.J., Tang, I.I., Greenberg, S.G., Williams, E.R., and Krantz, B.A. (2010). Structural basis for the unfolding of anthrax lethal factor by protective antigen oligomers. Nat Struct Mol Biol *17*, 1383–1390.

Finke, K., Plath, K., Panzner, S., Prehn, S., Rapoport, T.A., Hartmann, E., and Sommer, T. (1996). A second trimeric complex containing homologs of the Sec61p complex functions in protein transport across the ER membrane of S. cerevisiae. Embo J *15*, 1482–1494.

Finkelstein, A. (2008). Proton-coupled protein transport through the anthrax toxin channel. Philosophical Transactions of the Royal Society B: Biological Sciences.

Glynn, S.E., Martin, A., Nager, A.R., Baker, T.A., and Sauer, R.T. (2009). Structures of asymmetric ClpX hexamers reveal nucleotide-dependent motions in a AAA+ protein-unfolding machine. Cell *139*, 744–756.

Gmira, S., Karimova, G., and Ladant, D. (2001). Characterization of recombinant Bordetella pertussis adenylate cyclase toxins carrying passenger proteins. Res. Microbiol. *152*, 889–900.

Goloubinoff, P., and De Los Rios, P. (2007). The mechanism of Hsp70 chaperones: (entropic) pulling the models together. Trends Biochem. Sci. *32*, 372–380.

Herman, C., Prakash, S., Lu, C.Z., Matouschek, A., and Gross, C.A. (2003). Lack of a robust unfoldase activity confers a unique level of substrate specificity to the universal AAA protease FtsH. Mol. Cell *11*, 659–669.

Holubova, J., Kamanova, J., Jelinek, J., Tomala, J., Masin, J., Kosova, M., Stanek, O., Bumba, L., Michalek, J., Kovar, M., et al. (2012). Delivery of Large Heterologous Polypeptides across the Cytoplasmic Membrane of Antigen-Presenting Cells by the Bordetella RTX Hemolysin Moiety Lacking the Adenylyl Cyclase Domain. Infect Immun *80*, 1181–1192.

Hwang, W., and Lang, M.J. (2009). Mechanical design of translocating motor proteins. Cell Biochem. Biophys. *54*, 11–22.

Janowiak, B.E., Fischer, A., and Collier, R.J. (2010). Effects of introducing a single charged residue into the phe clamp of multimeric anthrax protective antigen. Journal of Biological Chemistry.

Jiang, Y., Cheng, Z., Mandon, E.C., and Gilmore, R. (2008). An interaction between the SRP receptor and the translocon is critical during cotranslational protein translocation. J. Cell Biol. *180*, 1149–1161.

Katayama, H., Janowiak, B.E., Brzozowski, M., Juryck, J., Falke, S., Gogol, E.P., Collier, R.J., and Fisher, M.T. (2008). GroEL as a molecular scaffold for structural analysis of the anthrax toxin pore. Nat Struct Mol Biol *15*, 754–760.

Kenniston, J.A., Baker, T.A., Fernandez, J.M., and Sauer, R.T. (2003). Linkage between ATP consumption and mechanical unfolding during the protein processing reactions of an AAA+ degradation machine. Cell *114*, 511–520.

Kenniston, J.A., Burton, R.E., Siddiqui, S.M., Baker, T.A., and Sauer, R.T. (2004). Effects of local protein stability and the geometric position of the substrate degradation tag on the efficiency of ClpXP denaturation and degradation. J. Struct. Biol. *146*, 130–140.

Kintzer, A.F., Thoren, K.L., Sterling, H.J., Dong, K.C., Feld, G.K., Tang, I.I., Zhang, T.T., Williams, E.R., Berger, J.M., and Krantz, B.A. (2009). The protective antigen component of anthrax toxin forms functional octameric complexes. J Mol Biol *392*, 614–629.

Krantz, B.A., Finkelstein, A., and Collier, R.J. (2006). Protein translocation through the anthrax toxin transmembrane pore is driven by a proton gradient. J Mol Biol *355*, 968–979.

Krantz, B.A., Melnyk, R.A., Zhang, S., Juris, S.J., Lacy, D.B., Wu, Z., Finkelstein, A., and Collier, R.J. (2005). A phenylalanine clamp catalyzes protein translocation through the anthrax toxin pore. Science *309*, 777–781.

Krantz, B.A., Trivedi, A.D., Cunningham, K., Christensen, K.A., and Collier, R.J. (2004). Acid-induced unfolding of the amino-terminal domains of the lethal and edema factors of anthrax toxin. J Mol Biol *344*, 739–756.

Kwon, A.-R., Trame, C.B., and McKay, D.B. (2004). Kinetics of protein substrate degradation by HslUV. J. Struct. Biol. *146*, 141–147.

Lacy, D.B., Wigelsworth, D.J., Melnyk, R.A., Harrison, S.C., and Collier, R.J. (2004). Structure of heptameric protective antigen bound to an anthrax toxin receptor: a role for receptor in pH-dependent pore formation. Proc Natl Acad Sci USA *101*, 13147–13151.

Lee, V.T., and Schneewind, O. (2002). Yop fusions to tightly folded protein domains and their effects on Yersinia enterocolitica type III secretion. J Bacteriol *184*, 3740–3745.

Leppla, S.H. (1982). Anthrax toxin edema factor: a bacterial adenylate cyclase that increases cyclic AMP concentrations of eukaryotic cells. Proc Natl Acad Sci USA *79*, 3162–3166.

Liu, Q., D'Silva, P., Walter, W., Marszalek, J., and Craig, E.A. (2003). Regulated cycling of mitochondrial Hsp70 at the protein import channel. Science *300*, 139–141.

Lizák, B., Csala, M., Benedetti, A., and Bánhegyi, G. (2008). The translocon and the non-specific transport of small molecules in the endoplasmic reticulum (Review). Mol. Membr. Biol. *25*, 95–101.

Mabry, R., Brasky, K., Geiger, R., Carrion, R., Hubbard, G.B., Leppla, S., Patterson, J.L., Georgiou, G., and Iverson, B.L. (2006). Detection of anthrax toxin in the serum of animals infected with Bacillus anthracis by using engineered immunoassays. Clin. Vaccine Immunol. *13*, 671–677.

Martin, A., Baker, T.A., and Sauer, R.T. (2005). Rebuilt AAA + motors reveal operating principles for ATP-fuelled machines. Nature *437*, 1115–1120.

Martin, A., Baker, T.A., and Sauer, R.T. (2008). Pore loops of the AAA+ ClpX machine grip substrates to drive translocation and unfolding. Nat Struct Mol Biol *15*, 1147–1151.

Matouschek, A., Pfanner, N., and Voos, W. (2000). Protein unfolding by mitochondria. The Hsp70 import motor. EMBO Rep. *1*, 404–410.

Melnyk, R.A., and Collier, R.J. (2006). A loop network within the anthrax toxin pore positions the phenylalanine clamp in an active conformation. Proc Natl Acad Sci USA *103*, 9802–9807.

Miller, C.J., Elliott, J.L., and Collier, R.J. (1999). Anthrax protective antigen: prepore-to-pore conversion. Biochemistry *38*, 10432–10441.

Milne, J.C., Furlong, D., Hanna, P.C., Wall, J.S., and Collier, R.J. (1994). Anthrax protective antigen forms oligomers during intoxication of mammalian cells. J Biol Chem *269*, 20607–20612.

Minamino, T., Morimoto, Y.V., Hara, N., and Namba, K. (2011). An energy transduction mechanism used in bacterial flagellar type III protein export. Nat Commun *2*, 475.

Movileanu, L., Schmittschmitt, J.P., Scholtz, J.M., and Bayley, H. (2005). Interactions of peptides with a protein pore. Biophys J *89*, 1030–1045.

Murphy, J.R. (2011). Mechanism of Diphtheria Toxin Catalytic Domain Delivery to the Eukaryotic Cell Cytosol and the Cellular Factors that Directly Participate in the Process. Toxins (Basel) *3*, 294–308.

Osborne, A.R., Rapoport, T.A., and van den Berg, B. (2005). Protein translocation by the Sec61/SecY channel. Annu. Rev. Cell Dev. Biol. *21*, 529–550.

Park, E., and Rapoport, T.A. (2011a). Mechanisms of Sec61/SecY-Mediated Protein

Translocation Across Membranes. Annu Rev Biophys.

Park, E., and Rapoport, T.A. (2011b). Preserving the membrane barrier for small molecules during bacterial protein translocation. Nature *473*, 239–242.

Petosa, C., Collier, R.J., Klimpel, K.R., Leppla, S.H., and Liddington, R.C. (1997). Crystal structure of the anthrax toxin protective antigen. Nature *385*, 833–838.

Pfanner, N., and Geissler, A. (2001). Versatility of the mitochondrial protein import machinery. Nat Rev Mol Cell Biol *2*, 339–349.

Ruprecht, M., Bionda, T., Sato, T., Sommer, M.S., Endo, T., and Schleiff, E. (2010). On the impact of precursor unfolding during protein import into chloroplasts. Mol Plant *3*, 499–508.

Sargent, F. (2007). The twin-arginine transport system: moving folded proteins across membranes. Biochem. Soc. Trans. *35*, 835–847.

Sauer, R.T., and Baker, T.A. (2011). AAA+ proteases: ATP-fueled machines of protein destruction. Annu Rev Biochem *80*, 587–612.

Schatz, G., and Dobberstein, B. (1996). Common principles of protein translocation across membranes. Science *271*, 1519–1526.

Schirmer, T., Keller, T.A., Wang, Y.F., and Rosenbusch, J.P. (1995). Structural basis for sugar translocation through maltoporin channels at 3.1 A resolution. Science *267*, 512–514.

Simon, S.M., Peskin, C.S., and Oster, G.F. (1992). What drives the translocation of proteins? Proc Natl Acad Sci USA *89*, 3770–3774.

Street, T.O., Lavery, L.A., and Agard, D.A. (2011). Substrate binding drives large-scale conformational changes in the Hsp90 molecular chaperone. Mol. Cell *42*, 96–105.

Striebel, F., Hunkeler, M., Summer, H., and Weber-Ban, E. (2010). The mycobacterial Mpa-proteasome unfolds and degrades pupylated substrates by engaging Pup's N-terminus. Embo J *29*, 1262–1271.

Sun, J., Lang, A.E., Aktories, K., and Collier, R.J. (2008). Phenylalanine-427 of anthrax protective antigen functions in both pore formation and protein translocation. Proc Natl Acad Sci USA *105*, 4346–4351.

Thoren, K.L., and Krantz, B.A. (2011). The unfolding story of anthrax toxin translocation. Mol Microbiol *80*, 588–595.

Thoren, K.L., Worden, E.J., Yassif, J.M., and Krantz, B.A. (2009). Lethal factor unfolding is the most force-dependent step of anthrax toxin translocation. Proc Natl Acad Sci USA *106*, 21555–21560.

Tomkiewicz, D., Nouwen, N., and Driessen, A.J.M. (2007). Pushing, pulling and trapping--

modes of motor protein supported protein translocation. Febs Letters *581*, 2820–2828.

van den Berg, B., Clemons, W.M., Collinson, I., Modis, Y., Hartmann, E., Harrison, S.C., and Rapoport, T.A. (2004). X-ray structure of a protein-conducting channel. Nature *427*, 36–44.

Wesche, J., Elliott, J.L., Falnes, P.O., Olsnes, S., and Collier, R.J. (1998). Characterization of membrane translocation by anthrax protective antigen. Biochemistry *37*, 15737–15746.

Wickner, W., and Schekman, R. (2005). Protein translocation across biological membranes. Science *310*, 1452–1456.

Woodhull, A.M. (1973). Ionic blockage of sodium channels in nerve. The Journal of General Physiology *61*, 687–708.

Yamano, K., Kuroyanagi-Hasegawa, M., Esaki, M., Yokota, M., and Endo, T. (2008). Step-size analyses of the mitochondrial Hsp70 import motor reveal the Brownian ratchet in operation. J Biol Chem *283*, 27325–27332.

Zhang, S., Cunningham, K., and Collier, R.J. (2004a). Anthrax protective antigen: efficiency of translocation is independent of the number of ligands bound to the prepore. Biochemistry *43*, 6339–6343.

Zhang, S., Udho, E., Wu, Z., Collier, R.J., and Finkelstein, A. (2004b). Protein translocation through anthrax toxin channels formed in planar lipid bilayers. Biophys J *87*, 3842–3849.